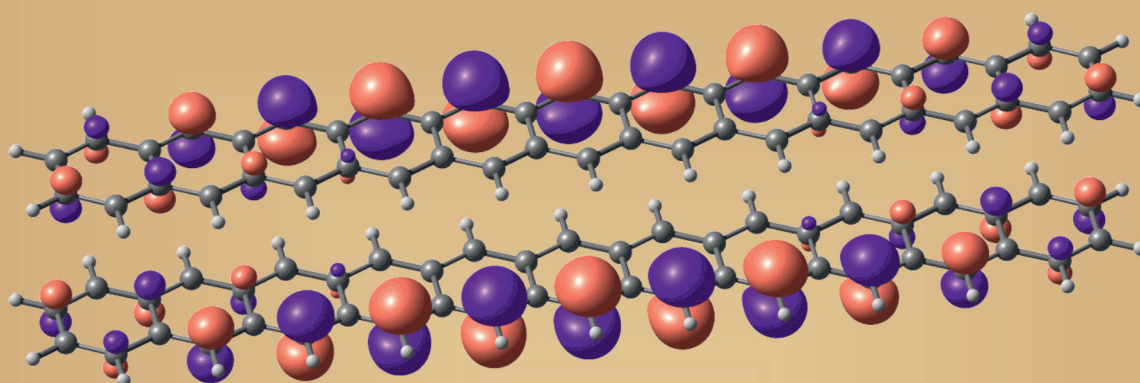


■ Fused-Ring Systems | *Reviews Showcase* |

Pushing the Limits of Acene Chemistry: The Recent Surge of Large Acenes

Christina Tönshoff and Holger F. Bettinger*^[a]

WANTED



The ACENES

Heptacene, Octacene, Nonacene, Decacene,
Undecacene, DodecaceneWanted for High Reactivity,
Extraordinary Electronic Structure,
and Frustration of Researchers

REWARD FAME AND FORTUNE

Abstract: Acenes, consisting of linearly fused benzene rings, are an important fundamental class of organic compounds with various applications. Hexacene is the largest acene that was synthesized and isolated in the 20th century. The next largest member of the acene family, heptacene, was observed in 2007 and since then significant progress in preparing acenes has been reported. Significantly larger acenes, up to undecacene, could be studied by means of low-temperature matrix isolation spectroscopy with in situ photolytic

generation, and up to dodecacene by means of on-surface synthesis employing innovative precursors and highly defined crystalline metal surfaces under ultrahigh vacuum conditions. The review summarizes recent experimental and theoretical advances in the area of acenes that give a significantly deeper insight into the fundamental properties and nature of the electronic structure of this fascinating class of organic compounds.

1. Introduction

Acenes are polycyclic aromatic hydrocarbons (PAHs) that consist of linearly fused benzene rings and have the general formula $C_{4N+2}H_{2N+4}$.^[1] A unique feature of acenes, which follows from this topology of ring fusion, is that they share only a single Clar sextet among all six-membered rings present (Figure 1).^[2–5]

This has dramatic consequences: acenes have the smallest energy gaps between the highest occupied and lowest unoccupied molecular orbitals (HOMO–LUMO gap) among PAHs of comparable size.^[6–10] A small HOMO–LUMO gap implies that the standard description of the electronic structure, involving only doubly occupied and fully vacant molecular orbitals (MOs), the picture that is deeply entrenched in the thinking of organic chemistry, cannot well represent acenes of a certain length. This was already realized in the 1980s^[11,12] and is today summarized as the radicaloid (or sometimes open-shell) character of acenes, which increases with length from diradicaloid to polyradicaloid.^[13–16] A hallmark of organic diradicals is the small singlet–triplet energy gap, ΔE_{ST} . To put the abstract wording of “diradicaloid character” of acenes into context, a comparison of pentacene, the largest acene for which ΔE_{ST} was determined experimentally, with a typical organic diradical, *m*-benzynes, is instructive: both have an energy gap, ΔE_{ST} , of roughly 20 kcal mol^{−1} (Figure 2).^[17,18] The small HOMO–LUMO energy differences of acenes cause small optical gaps, energetically low-lying triplet states, low ionization potentials (IPs), and high electron affinities (EAs).^[19–21]

These special properties make some members of the acene family, in particular, tetracene and pentacene, of high impor-


ance for applications.^[22–26] Pentacene is a superb hole transporting (i.e., p-channel) semiconductor, and hence, the compound is of high relevance in organic field-effect transistor (OFET) research. Its excited-state ordering $E(S_1) > 2E(T_1)$ turned it into a test subject in singlet fission research.^[27–29]


The flipside of the coin is that the electronic structural features outlined above also cause high reactivity. Indeed, because acenes only have one Clar sextet, they are the most reactive among PAHs of a similar size. The kinetic stability of acenes decreases with an increasing number of rings because they tend to dimerize (or possibly polymerize)^[30,31] and react readily with oxygen, especially in solution.^[32,33] Consequently, the largest acene that could be synthesized in the 20th century through conventional organic chemistry techniques was hexacene (**6ac**).^[33–40] Although this could be structurally characterized by using single-crystal X-ray diffraction,^[40,41] as well as by a number of spectroscopy techniques,^[20,33–40,42,43] solution-phase NMR spectroscopy was not reported for **6ac**. This is due to an additional problem of acene chemistry: due to high CH– π intermolecular interaction energies of adjacent molecules in the herringbone crystal structure, solubility is very low for the larger members.


These problems could successfully be alleviated, to a certain extent, by the introduction of trialkylsilylethynyl (R_3SiC_2-) substituents that increase stability and solubility at the same time. Following pioneering work on 6,13-di(triisopropylsilylethynyl)-pentacene,^[44,45] it was possible to synthesize stabilized hexacenes,^[46,47] heptacenes,^[46,48–50] and even nonacenes.^[51,52] The substituted heptacenes could be characterized spectroscopically and structurally, and it was shown that they had significant persistence in solution.^[46,48–50] The nonacene derivatives could be characterized by means of optical spectroscopy and single-crystal X-ray analysis, but solution-phase NMR spectroscopy was precluded.^[52] The authors found that the quality of the ¹H NMR spectra improved with the deterioration of the nonacene derivatives, and it is possible that this is due to the presence of nonacene high-spin species, such as radical ions generated by photoredox processes or thermally populated triplet nonacenes, as a consequence of the energetically close-lying triplet state. Larger kinetically stabilized acenes have not been reported, to date.

The ground-breaking 2006 paper of Neckers et al., which first provided convincing evidence for the existence of heptacene (**7ac**) by means of polymer matrix isolation at room tem-

[a] Dr. C. Tönshoff, Prof. Dr. H. F. Bettinger
Institut für Organische Chemie, Universität Tübingen
Auf der Morgenstelle 18, 72076 Tübingen (Germany)
E-mail: holger.bettinger@uni-tuebingen.de

 The ORCID identification number(s) for the author(s) of this article can be found under:
<https://doi.org/10.1002/chem.202003112>.

 © 2020 The Authors. Published by Wiley-VCH GmbH. This is an open access article under the terms of the Creative Commons Attribution Non-Commercial License, which permits use, distribution and reproduction in any medium, provided the original work is properly cited and is not used for commercial purposes.

 Selected by the Editorial Office for our Showcase of outstanding Review-type articles (www.chemeurj.org/showcase).

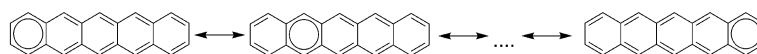


Figure 1. Clar resonance structures of pentacene.

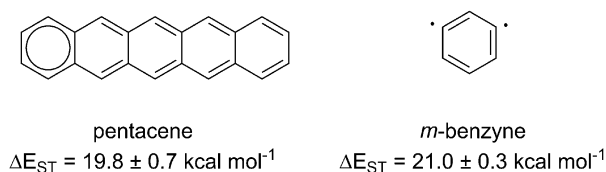


Figure 2. Singlet–triplet energy gaps measured for pentacene^[17] and *m*-benzyne.^[18]

perature,^[53] was quickly backed by more detailed cryogenic matrix isolation investigations,^[54,55] and thus, significant advances were achieved in the preparation of unsubstituted long acenes. The key to success of all new studies is the generation of the acene under investigation from suitable precursors within the vacuum system of the experimental setup. In this way, octacene (**8ac**) and nonacene (**9ac**) could be observed spectroscopically in 2010 under cryogenic matrix isolation conditions.^[56] Nonetheless, it took several years until larger systems were successfully studied.

Today, undecacene (**11ac**; Figure 3) is the largest acene that has been studied experimentally by our research group under matrix isolation conditions,^[57] and by Echavarren et al. by means of on-surface synthesis.^[58] The on-surface generation of acenes, combined with state-of-the-art microscopy techniques, has seen a significant boost over the last few years, and the field quickly achieved the investigation of acenes up to dodecacene (**12ac**; Figure 3), which is the longest acene observed so far.^[59] Herein, we summarize recent developments of research into (parent) acenes larger than pentacene.

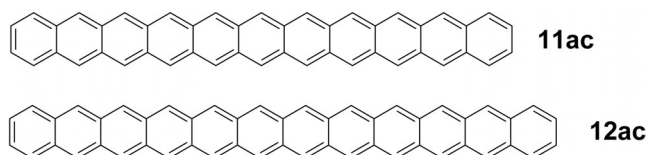


Figure 3. Structures of undecacene (**11ac**) and dodecacene (**12ac**), which are the longest acenes observed, so far.

2. Hexacene and Heptacene in Bulk Phases

Although the first synthesis of hexacene (**6ac**) was already reported in 1939,^[34] its high reactivity has limited detailed investigations and applications, as reviewed by us in 2014.^[60,61] The decarbonylation route to **6ac** (Scheme 1a) introduced by the group of Chow^[62] employs a precursor strategy that allows the generation of **6ac** in a convenient manner.^[40] Single crystals of this material were employed in field-effect transistors and resulted in averaged mobilities of $0.88 \text{ V cm}^{-2} \text{ s}^{-1}$, whereas the best hole mobility observed was $4.28 \text{ cm}^2 \text{ V}^{-1} \text{ s}^{-1}$. Watanabe

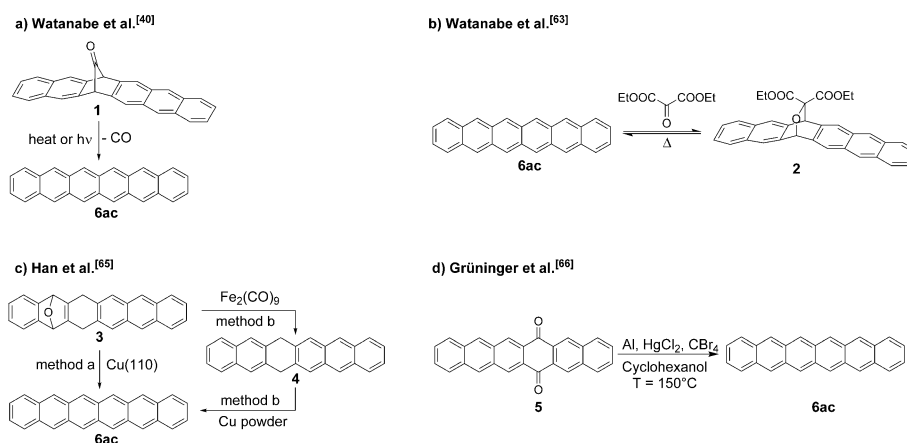
et al. subjected **6ac** to a Diels–Alder reaction with diethyl malonate under microwave conditions, and from the cycloaddition adduct, **6ac** could be generated after annealing in a nitrogen atmosphere at 240°C (Scheme 1b).^[63] In this way, it was possible to obtain films of **6ac** by means of spin coating and to fabricate OFET devices that showed low hole mobility, which was suggested to result from the low quality of the films.^[63] The best results obtained after optimization were $3.5 \times 10^{-2} \text{ cm}^2 \text{ V}^{-1} \text{ s}^{-1}$.^[63] The same group also used **6ac** obtained by the decarbonylation route for the fabrication of OFETs by means of vacuum deposition and obtained a hole mobility of $7.6 \times 10^{-2} \text{ cm}^2 \text{ V}^{-1} \text{ s}^{-1}$.^[64] Interestingly, 2-bromohexacene, which was obtained from an analogous thermal precursor, formed smoother films and showed an eightfold higher hole mobility of $0.83 \text{ cm}^2 \text{ V}^{-1} \text{ s}^{-1}$.^[64]

Han et al. also investigated the semiconductor performance of **6ac** in OFET devices.^[65] They synthesized **6ac** through dehydrogenation of 6,15-dihydrohexacene (**4**) with copper powder during sublimation.^[65] This was the same method that Clar used in the first synthesis of **6ac** back in 1939,^[34] although he obtained **4** in a different way. For OFET fabrication, compound **6ac** was deposited by means of vacuum sublimation onto surface-modified SiO_2 (polymers and self-assembled monolayers) gate electrodes.^[65] The best results were obtained for the polystyrene (PS) dielectric layer with $\mu = 0.123 \text{ cm}^2 \text{ V}^{-1} \text{ s}^{-1}$.^[65] A photograph of solid **6ac** given by Han et al. (Figure S1a of ref. [65]) showed a turquoise color, whereas Watanabe et al. obtained a dark-blue solid (Figure 2a of ref. [40]). The sample of **6ac** that

Christina Tönshoff studied chemistry at Ruhr-University Bochum, Germany, and received her doctoral degree from this university in 2004 under the guidance of Dr. Götz Bucher. After graduation, she joined the Bettinger research group in Bochum and moved to Tübingen in 2008. Her research interests are polycyclic aromatic hydrocarbons, in particular, acenes, and reactive intermediates, which she investigates with matrix isolation and computational quantum chemistry methods.

Holger Bettinger studied chemistry at the Friedrich-Alexander University Erlangen-Nuremberg, Germany, and received his doctoral degree under the guidance of Prof. Dr. P. v. R. Schleyer in 1998. He conducted postdoctoral research at the University of Georgia (Athens, GA, USA) and Rice University (Houston, TX, USA). His habilitation at the Ruhr-University Bochum, Germany (2005, mentor Prof. Dr. W. Sander), was supported by a Liebig Fellowship. He became Heisenberg Fellow in 2006 and accepted his current position at the University of Tübingen in 2008. He is author of 150 papers in the areas of reactive polycyclic aromatic hydrocarbons, boron–nitrogen-substituted aromatic compounds, carbonaceous materials, and boron and boron–nitrogen analogues of organic reactive intermediates.





Scheme 1. Recent syntheses of hexacene (**6ac**).

we obtain after sublimation (see below) has an appearance similar to that of the sample of Watanabe et al.,^[40] while remaining turquoise-colored residual materials are discarded. This suggests that the purity of the samples of Han et al.^[65] could be further improved, which, in turn, could result in better performing devices being obtained.

The photophysics of films and crystals of **6ac** was also investigated.^[43] Hexacene was obtained through the decarbonylation route (Scheme 1a), and from ultrafast dynamics, it was concluded that, due to the dominant singlet fission relaxation pathway ($S_1 \rightarrow 2 \times T_1 + \text{photons}$), **6ac** was suboptimal for photovoltaics because some of the energy was dissipated as heat.^[43] Another unexpected observation was that singlet fission of **6ac** was very efficient, but slower than that in pentacene. A somewhat simplified explanation is associated with an energy gap law: the larger energy gap between S_1 and $2 \times T_1$ in **6ac**, compared with that of pentacene, reduces the singlet fission rate.^[43]

Films of **6ac** on Au(110) were prepared, and the thin-film properties and electronic structure of **6ac** were investigated by using X-ray photoelectron spectroscopy (XPS) and X-ray absorption spectroscopy (XAS) by Grüniger et al.^[66] The required **6ac** was obtained through Meerwein–Ponndorf–Verley (MPV) reduction of 6,15-hexacenequinone followed by sublimation for purification (Scheme 1d). The advantage of this route is that 6,15-hexacenequinone is readily available on a multigram scale and that MPV reduction is straightforward. This outweighs, in our view, the low yield of high-purity **6ac** after gradient sublimation (1% initially, but about 10% after improvements).^[66] The compound was subsequently employed in organic vapor-phase deposition, as performed routinely with other organic semiconductors. It was concluded that the molecules of **6ac** adopted an almost flat-lying arrangement at the **6ac**–Au(110) interface.^[66] In addition, the thickness dependence of the X-ray absorption spectra suggests that there is strong coupling of molecular states with the states of the Au(110) substrate.^[66]

The electronic interface properties and molecular orientation of **6ac** on oxygen-terminated copper, Cu(110)–(2 × 1)O, was

also investigated by using XAS and XPS, respectively.^[67] The molecules align with their long axis parallel to the oxygen row, while the short axis is tilted with respect to the substrate (Figure 4).^[67] This shows that the Cu(110)–(2 × 1)O surface can be used as a template for film growth of **6ac** up to a thickness of at least 16 nm.^[67]

The first attempts at the synthesis of heptacene (**7ac**) date back to 1942.^[68] However, the first convincing evidence for its existence was provided by the group of Neckers in 2006 (see above) by means of polymer matrix isolation.^[53] The question of whether **7ac** could only exist in matrices was addressed by our research group in 2017.^[69] MPV reduction of 7,16-heptacenequinone (**6**) does not result in **7ac**, but rather in two isomers of diheptacene (**7a** and **7b**) that could not be separated (Scheme 2).

Attempted sublimation of the **7** under high-vacuum conditions resulted in sublimation of monomeric **7ac**, as shown by means of cryogenic argon matrix isolation. Deposition of vapor

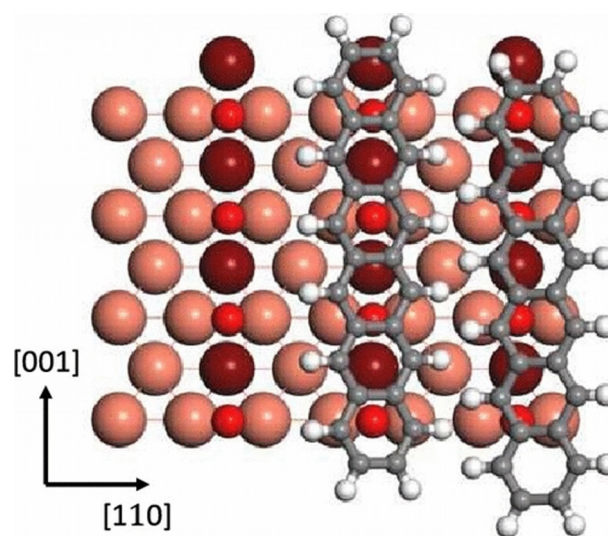
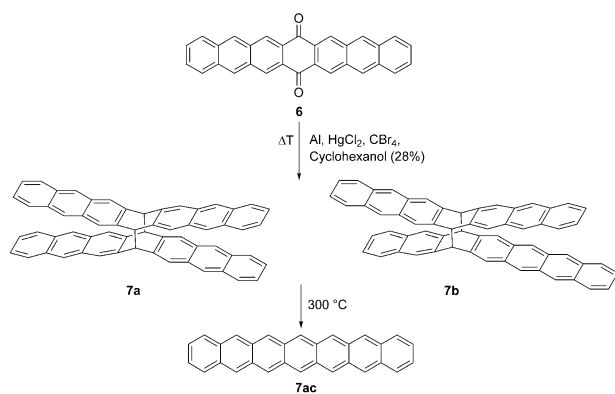


Figure 4. The orientation of **6ac** on a Cu(110)–(2 × 1)O surface. Reproduced with permission.^[67] Copyright 2018, American Chemical Society.



Scheme 2. MPV reduction of **6** produces **7a** and **7b** that undergo thermally induced cyclization to **7ac** upon heating.^[69]

of **7ac** in the absence of argon allowed growth of films of **7ac**, as evidenced by optical spectroscopy. Although partial decomposition cannot be ruled out, the persistence of these films at room temperature and under high vacuum clearly demonstrate that **7ac** can exist in the bulk phase for some time. The

most convincing evidence comes from solid-state cross polarization magic angle spinning (CPMAS) ¹³C NMR spectroscopy (Figure 5). Heating of sample **7** in a rotor commonly used for solid-state NMR spectroscopy to 300 °C for 10 min shows that the ¹³C signals associated with tetrahedral bridgehead carbon atoms at $\delta = 54.7$ ppm essentially disappear, whereas the spectrum in the range of the aromatic carbon atoms changes (signals at $\delta = 138.3, 130.3, 126.2, 122.7$ ppm decrease) and adopts the shape expected for **7ac** ($\delta = 129.4, 126.6$ ppm, with a shoulder at $\delta \approx 124$ ppm). The thermal cleavage of dimers appears to be reversible because some of the initial signals due to the bridgehead carbon atoms of **7** grow over some time. Another heating cycle, however, regenerates **7ac**.

The decarbonylation route was also extended to **7ac** (Scheme 3), as well as to isomeric dibenzopentacenes.^[70] The synthesis employed ketone-protected bis-diene **8**, which was used in Diels–Alder reactions with 2,3-didehydronaphthalene, aromatized, deprotected, and finally decarbonylated. The decarbonylation reaction sets in at 205 °C, according to thermogravimetric analysis and **7ac** is found to be stable up to 420 °C.^[70]

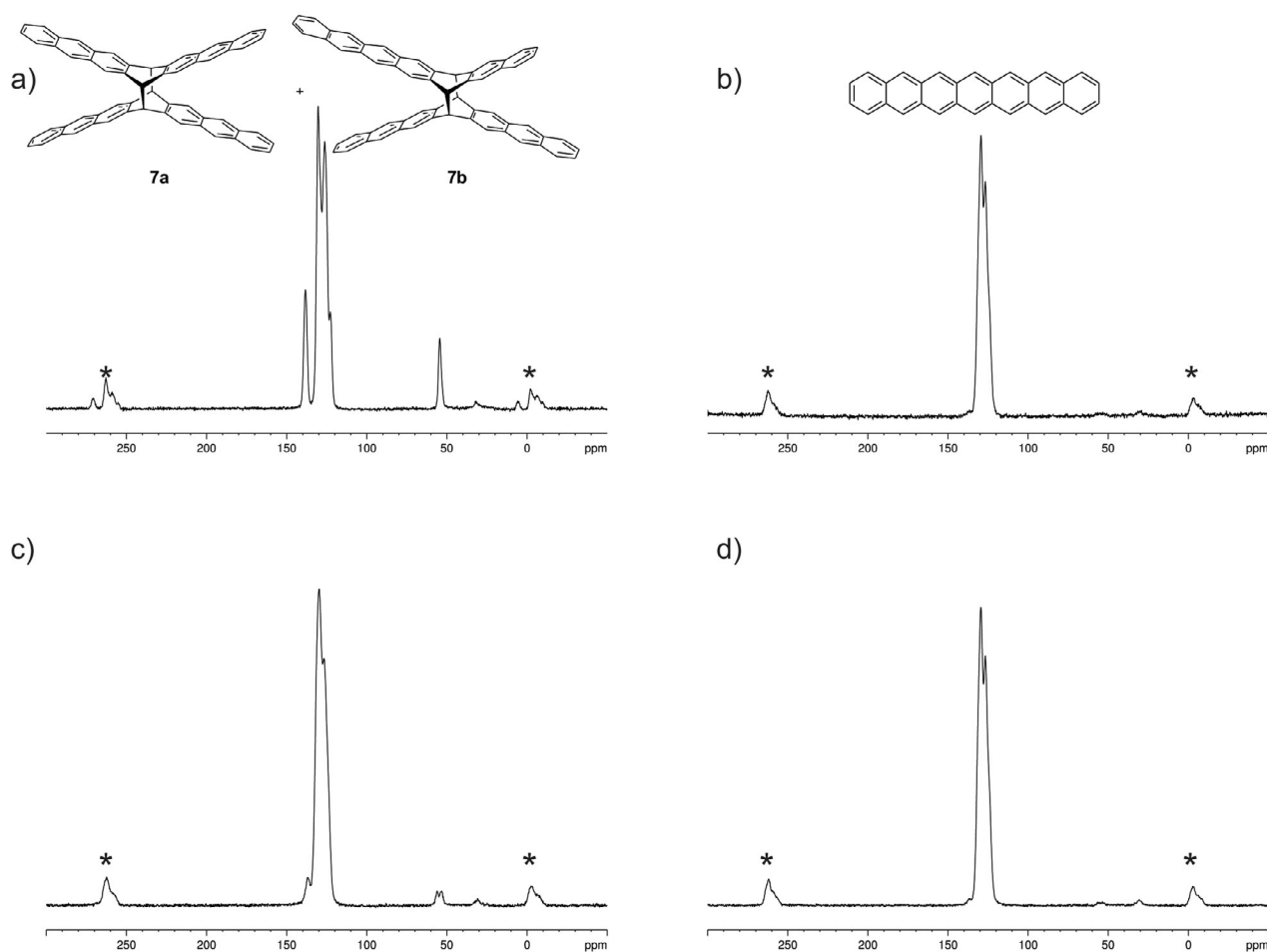
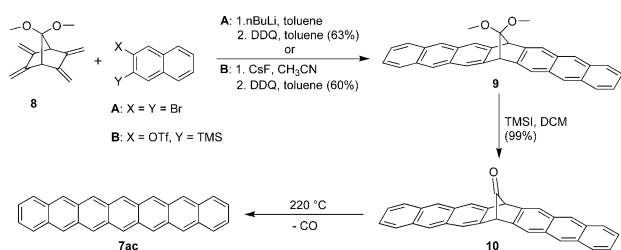


Figure 5. Solid-state CP-MAS ¹³C NMR spectra. a) Product mixture obtained after MPV reduction of **6**. b) Heptacene (**7ac**) obtained after heating to 300 °C for 12 min. c) Sample from b) after one month at room temperature under an ambient atmosphere. d) Same sample after heating again (300 °C/12 min). (Asterisks mark rotational side bands.) Reproduced with permission.^[69] Copyright 2017, American Chemical Society.



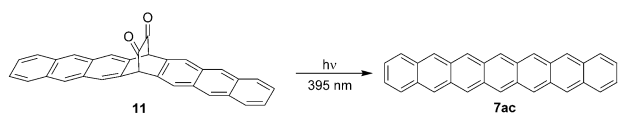
Scheme 3. Decarbonylation route to **7ac**. DDQ = 2,3-dichloro-5,6-dicyano-1,4-benzoquinone, OTf = triflate, TMS = trimethylsilyl, DCM = dichloromethane.^[70]

The sample of **7ac** was characterized by means of IR and solid-state CP-MAS ¹³C NMR spectroscopy and high-resolution ESI-MS.^[70] The authors stressed the prospects of using this technique for solid-state synthesis of larger acenes,^[70] which, in view of the work of Fang on **8ac** and **9ac**,^[71] seems to be plausible.

3. Preparation of Large Acenes under Matrix Isolation Conditions

As mentioned above, the first convincing evidence for the existence of heptacene (**7ac**) was provided by the group of Neckers in 2006, using matrix isolation techniques.^[53] Employing a poly(methyl methacrylate) (PMMA) matrix at room temperature, photolysis of α -diketone **11** with a light-emitting diode (LED) resulted in photodecarbonylation (Strating–Zwanenburg^[72–75] reaction) and formation of **7ac** (Scheme 4). Phototransformation in PMMA at room temperature was monitored by means of UV/Vis spectroscopy,^[53] and subsequently also in noble-gas cryogenic matrixes by means of IR and UV/Vis spectroscopy,^[54,55] and showed the clean formation of **7ac**.

At 10 K, noble-gas matrix isolated **7ac** is not EPR active (see the discussion on diradical character below) and does not thermally react with dioxygen upon annealing up to 35 K.^[54,55] At room temperature and under an ambient atmosphere, the PMMA-embedded sample of **7ac** was stable for up to 4 h, but degraded due to reaction with atmospheric oxygen, which could diffuse into the polymer. Indeed, the oxygen-induced bleaching of **7ac** was used to measure the oxygen permeability of polymers.^[76] A comparison of these results with the behavior of solid **7ac**, which appears to be stable for weeks,^[69,70] shows that solid-state aggregation enhances the stability dramatically. Similar differences in stability were reported for **6ac**, which could not be synthesized by photogeneration from its α -diketone precursor in solution due to photolability under the conditions of its generation,^[33] and only had a short life-



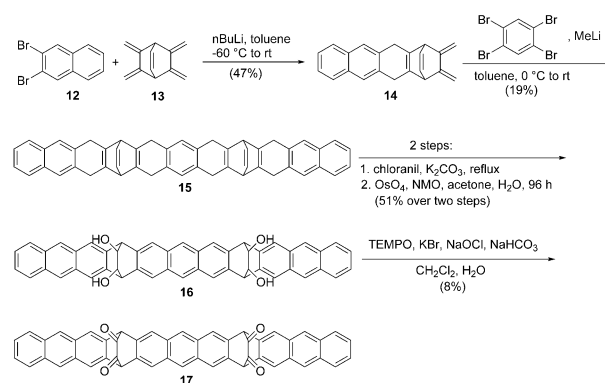
Scheme 4. Synthesis of **7ac** through photodecarbonylation (Strating–Zwanenburg reaction).

time of about 5 min in solution,^[63] but was stable for months in the solid state.^[40]

The experimental strategy to produce the target acene from the α -diketone precursor through photoirradiation by the Strating–Zwanenburg reaction was earlier applied for the synthesis of pentacene in toluene by Yamada et al.,^[77,78] and since has been employed successfully for the photogeneration of acenes.^[79] This strategy was also adopted for studying **6ac** and **7ac**, but, due to their instability towards oxidation and dimerization in solution during irradiation, photolysis was performed in both polymer matrices and noble-gas matrices.^[33,53–55] The method turned out to be more broadly applicable and has been successfully applied to acenes as large as **8ac**,^[56] **9ac**,^[56] and **11ac**.^[57] To obtain **8ac** and **9ac**, it was necessary to include a second α -diketone bridge in the precursor molecules. Otherwise the precursors were deemed to be too unstable because they would contain tetracene units themselves. With these precursors in hand, **8ac** and **9ac** could be observed in an argon matrix,^[56] as reviewed by us previously.^[60,61]

The next step was the preparation of **11ac**.^[57] The synthesis of the precursor followed the strategy established previously,^[56] which was based on repeated Diels–Alder reactions between in situ generated arynes and core building block **13** with two diene moieties, and provided access to the undecacene scaffold **15** (Scheme 5). After aromatization, dihydroxylation by OsO₄ and oxidation by using TEMPO/NaOCl tetraketone **17** was obtained.

The synthesis is very challenging and only small amounts of undecacene precursor **17** were obtained. The synthesis of the missing decacene (**10ac**) by an analogous reaction sequence would be even more demanding because systems with an even number of rings require an additional Diels–Alder step. However, synthetic availability is not the only problem that hampers the study of larger polyacenes. It turned out that undecacene precursor **17** could not be sublimed without decomposition, so isolation in an inert-gas matrix was not successful. Instead, it was prepared in a polymer matrix on top of an optical window. In contrast to smaller acenes, up to **7ac**, which could be studied in polymers at room temperature, photolysis



Scheme 5. Synthesis of photoprecursor **17** used for the preparation of **11ac**. NMO = *N*-methylmorpholine *N*-oxide, TEMPO = (2,2,6,6-tetramethylpiperidin-1-yl)oxyl.

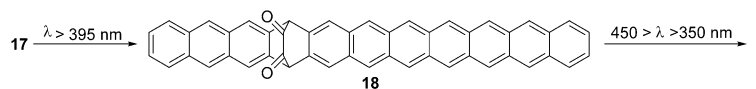
was performed at 8 K under high vacuum, and the reaction progress was studied by means of UV/Vis spectroscopy.

Because acenes possess very characteristic electronic absorption spectra,^[80] UV/Vis spectroscopy is a highly suitable method for their characterization, especially under matrix isolation conditions that generally preclude more conventional organic chemistry analytical tools. The optical spectra of the smaller acenes are textbook examples.^[80] Their spectra generally show three band systems, called β , α , and p bands, according to Clar (or 1B_g , 1L_b , and 1L_a , according to Platt). The β band is of high intensity, whereas the α band is very weak. The p band has an intermediate intensity. It often shows a characteristic vibrational fine structure and is associated with the HOMO to LUMO transition, and thus, the optical gap. Both the β and p bands are shifted bathochromically with increasing size of the acene system. A detailed analysis of the optical spectra of acenes up to **6ac**^[20] was provided by Nijegorodov et al.^[21]

The gradual evolution of the optical spectra with increasing acene length, up to **9ac**, strongly suggests that this compound still has a singlet electronic ground state, in contrast to the expectation based on extrapolation from data available up to **6ac**.^[20] The singlet nature of the acene series is supported by the available computational quantum chemistry results (see below). The optical spectra become more complicated with increasing acene size as new strong bands appear, which, according to DFT/multireference configuration interaction (MRCI) calculations,^[81] arise from two-electron transitions that become increasingly important for the larger systems. One of these transitions, called D2,^[81] gains significantly in intensity and falls faster in energy than the β band.

The formation of **11ac** proceeds in a stepwise manner,^[57] as also observed for the formation of **8ac** and **9ac** from their respective photoprecursors.^[56] Cleavage of the first α -diketone bridge ($\lambda > 395$ nm) results in the formation of **18** (Scheme 6), with a heptacene subunit, showing a strong absorption at 354 nm and a band system of low intensity with maxima at 707, 783, and 805 nm (p band; see Figure 6, bands with arrows pointing downward). The second α -diketone bridge is cleaved by prolonged irradiation with shorter wavelength in the range 350–450 nm,^[57] and two new absorptions are observed, a strong band with a maximum at $\lambda = 543$ nm that is assigned to the D2 state and a very weak band at $\lambda = 1007$ nm, corresponding to 1.23 eV. This band is assigned as the p band.^[57]

Taking into account the bathochromic shift due to the matrix material (bands are shifted bathochromically in PS compared with those in argon), a limiting optical gap of 1.2 eV for an infinite chain length is obtained by exponential extrapolation (Figure 7).



Scheme 6. Photolysis of **17** in a PS matrix at 8 K.

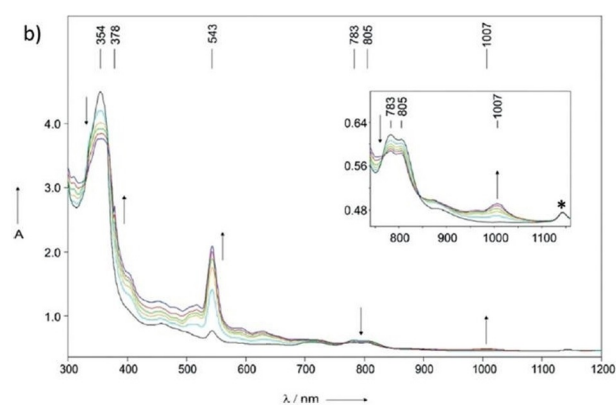


Figure 6. Spectrum obtained after successive irradiation of **17** in PS at 8 K with light of wavelengths $\lambda > 395$ nm and then $450 > \lambda > 350$ nm (arrows pointing upward or downward indicate the increase or decrease of the bands after irradiation; * marks a PS absorption). Reproduced with permission,^[57] Copyright 2018, Wiley-VCH.

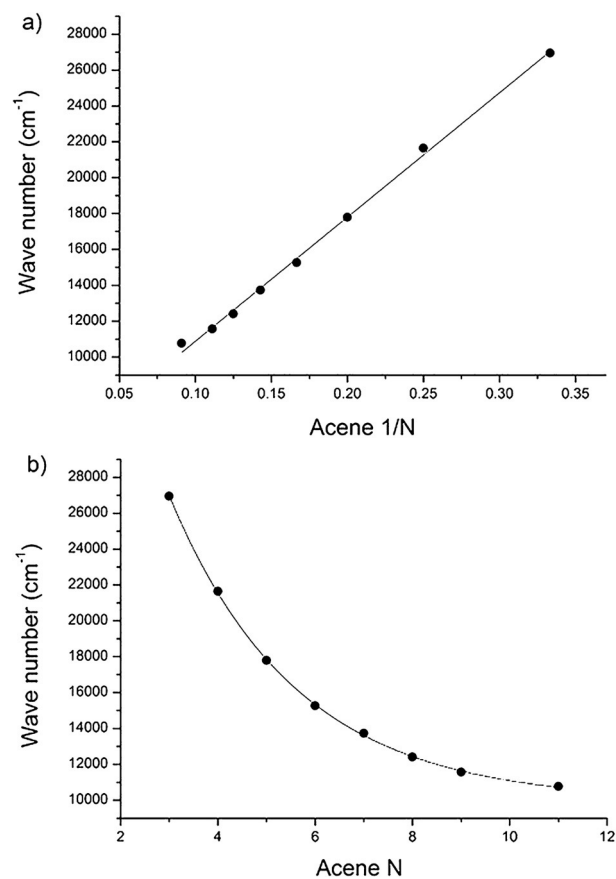


Figure 7. a) Plot of the energy maximum of the p band (HOMO \rightarrow LUMO) transition in the acene series; N = number of condensed benzene rings. b) Exponential fit ($y = 9923 \text{ cm}^{-1} + 53873 \text{ cm}^{-1} \times e^{-x/2.609}$) of the transition energies; $R^2 = 0.9998$. Reproduced with permission,^[57] Copyright 2018, Wiley-VCH.

4. On-Surface Studies

Highly reactive molecules can be prepared on inert surfaces under ultrahigh vacuum (UHV) conditions at cryogenic temperatures from suitable precursors. The great advantage of these techniques is that sophisticated detection methods allow the imaging of individual molecules and the investigation of electronic properties and molecular orientations.

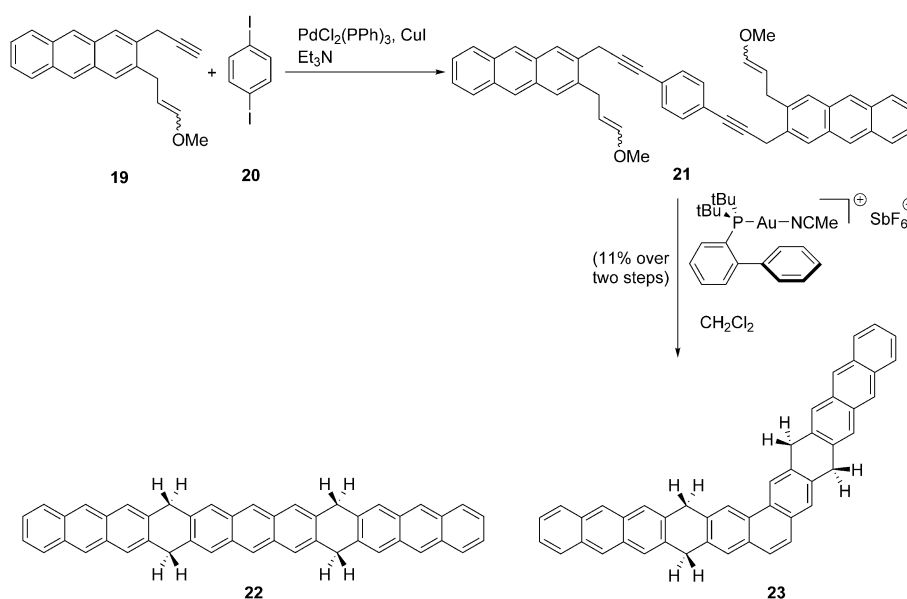
The scanning probe techniques of scanning tunneling microscopy and spectroscopy (STM/STS) and noncontact (nc) AFM provide complementary information about the molecular properties.^[82,83] During recent decades, significant progress has been made in the development of these techniques. A breakthrough was the development of controlled tip functionalization.^[84,85] For the study of organic molecules, CO termination turned out to be highly useful in yielding images of high resolution, as shown for the first time in 2009 in the study of pentacene on Cu(111), which revealed the atomic structure and bonding situation of a single molecule adsorbed on the surface by means of nc-AFM.^[86] Whereas AFM gives an insight into the atomic structure of a molecule, such as the atomic connectivity and bonding situation, STM allows information about the electronic properties to be obtained. In STM methods, depending on the bias voltage, electrons can tunnel from the tip to the LUMO of the organic molecule or from the HOMO of the molecule to the tip. Differential conductance, dI/dV , is related to the local density of states (LDOS), which, in distinct organic molecules, can be described in terms of molecular orbitals. Plotting differential conductance, dI/dV , versus bias voltage, V_{bias} , allows the determination of the STM transport gap, ΔV_{STM} , which is not exactly equal to the optical gap or the HOMO–LUMO gap, since the tunneling process results in temporarily charging the molecule (adding or removing an electron). Spatially resolved dI/dV maps at a given bias voltage produce images of electron density that can be related to fron-

tier orbitals if tunneling is dominated by a single channel as LDOS are related to the square of the electronic wavefunction.

For the synthesis of oligoacenes on surfaces, three different reactions were employed: 1) dehydrogenation of hydroacenes, 2) deoxygenation of epoxyacenes, and 3) decarbonylation of α -diketones. On-surface generation research has been conducted during the last three years and today all acenes up to **12ac** can be characterized on surfaces. The majority of studies used gold or silver single crystals as substrates. The influence of the substrate nature (e.g., Au, Ag, or Cu) and symmetry (e.g., Au(111) or Au(110)) on the chemical processes was reviewed.^[87] The interaction of organic materials with Au is generally weaker than that with Ag or Cu, and the hexagonal (111)-oriented surfaces are the densest and most inert, whereas the rectangular (110)-oriented surfaces are least dense and most reactive.^[87]

4.1. Dehydrogenation of tetrahydroacenes

In 2017, Zuzak et al. reported the generation of **9ac** from tetrahydrononacene and in 2018 they described the preparation of the entire series from **7ac** to **11ac**.^[58,88] The key steps in the synthesis of the tetrahydroacene precursors, shown in Scheme 7 for the undecacene system, are Sonogashira coupling reactions between alkynes, such as **19** and 1,4-diiodobenzene (**20**).^[58,89] The obtained dienyne undergo a double gold(I)-catalyzed cyclization that leads to a mixture of the desired linear and angular precursors **22** and **23**. For the smaller precursors with seven, eight, or nine annulated rings, the corresponding two acene and phene isomers can be separated due to their differing solubility. In case of the formation of **10ac** and **11ac**, these mixtures were used directly, exploiting the advantage of surface imaging techniques that allow studying individual molecules.^[58]



Scheme 7. Synthesis of hydrogenated precursors **22** and **23** used for the preparation of **11ac** and undecaphene.^[58]

The acenes can be generated on Au(111) either by tip-induced, stepwise hydrogen abstraction or by annealing, as shown by Zuzak et al. in their detailed study of **9ac**.^[88] In the tip-induced method, the tip is placed successively above the methylene bridges and a bias voltage higher than that of the value corresponding to the LUMO is applied. The process can be followed by means of both high-resolution, constant-height nc-AFM and filled- and empty-state STM topographies of **25a** and **9ac** can be observed. Annealing allows the preparation of larger amounts of **9ac** and the outcome depends on temperature. Whereas at 210 °C complete dehydrogenation yielding **9ac** is observed, at lower temperatures of about 150 °C partial dehydrogenation takes place, which is accompanied by hydrogen migration, and thus, leads to a mixture of dihydrononacenes, with 8,19-dihydrononacene (**25b**) as the main isomer (Scheme 8).

The electronic properties were studied by means of STS, as shown in Figure 8.^[88] Differential conductance spectra for the filled-state regime (hole tunneling) show resonances at -0.34 , -1.0 , and -1.65 V, corresponding to HOMO, HOMO–1, and HOMO–2, respectively. In the empty-state measurement (electron tunneling), the two detected peaks at $+0.85$ and $+1.7$ V are attributed to LUMO and LUMO+1, respectively. In this way, a HOMO–LUMO gap of 1.19 eV is obtained for the molecule of **9ac**, as illustrated in Figure 8a. Peak assignment was corroborated by dI/dV mapping at voltages corresponding to the resonances. They coincide with calculated maps and show the characteristic features of the corresponding orbitals.

Zuzak et al. also describe the formation of all acenes from **7ac** to **11ac** on Au(111).^[58] In one of the experiments, they deposited the hydrogenated precursors of **7ac**, **8ac**, **10ac**, and decaphene as a mixture onto the Au(111) surface and prepared the acenes efficiently through annealing. Different acenes can be detected separately at different spots on the surface and again nc-AFM with a CO-modified tip is used to obtain submolecularly resolved images. The authors mention the weak binding of planar acenes to the substrate through van der Waals type interactions, which lead to high mobility and the possibility of an easy displacement of molecules at moderate bias voltage and low tunneling currents. Immobilization seems to become more difficult with increased length of the acene, so

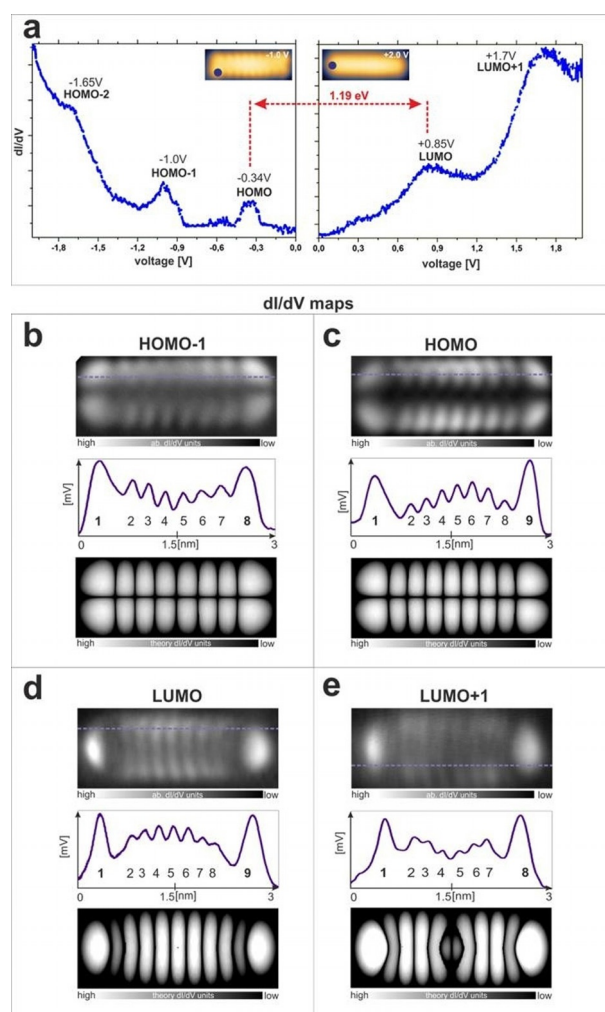
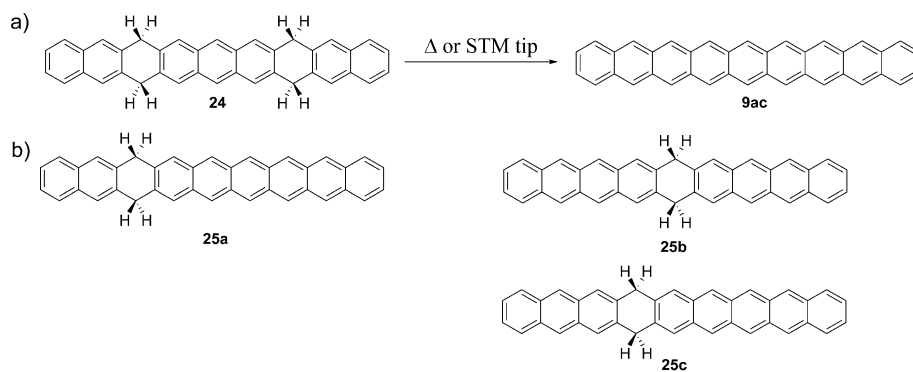


Figure 8. a) Single-point STS data recorded over a molecule of **9ac**. Insets show the lateral tip position during the acquisition of filled- (left panel, 100 pA) and empty-state (right panel, 50 pA) spectroscopy data. b)–e) Experimental dI/dV spatial maps recorded at energies corresponding to resonances shown in a) complemented by theoretically calculated maps; cross sections along experimental maps are displayed to guide the eye in symmetry analysis; tunneling current: 100 (b,c) and 50 pA (d,e). Reproduced with permission.^[88] Copyright 2017, American Chemical Society.



Scheme 8. a) On-surface synthesis of nonacene (**9ac**) and b) partially dehydrogenated intermediates: **25a** is observed in both thermal or tip-induced processes, and **25b** (main isomer) and **25c** are observed during annealing.^[88]

that the imaging of **10ac** is very challenging and succeeds for a molecule that is immobilized in the vicinity of a surface step. It was suggested that the increased length hindered “location between the elevated surface reconstruction rows.”^[58]

The longest acene prepared on an Au(111) surface in the study by Zuzak et al. was **11ac**.^[58] The mixture of linear and angular precursors **22** and **23** (Scheme 7) for **11ac** and undecaphene was used for deposition on the surface, and the image revealed smaller fragments, which were probably produced during the deposition process because the stability of the precursor decreased with an increasing number of annulated rings. This again emphasizes the difficulties and challenges in preparing large acenes. As for the smaller acene members, **11ac** can be prepared from the hydrogenated precursor by means of either tip-induced dehydrogenation or annealing (520 K). Figure 9 shows on-surface-generated **11ac** and its kinked isomer obtained after annealing, as observed by means of empty-state STM and nc-AFM. The AFM image reveals the structure with 11 linearly fused benzene rings in **11ac**. From STS measurements, the filled- and empty-state values of **11ac**

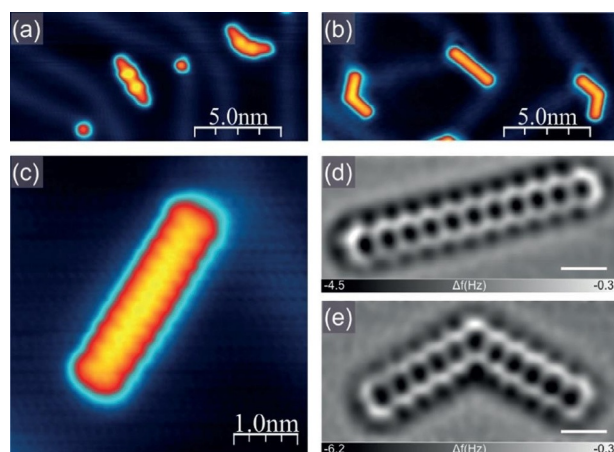


Figure 9. On-surface generation of **11ac**. Empty-state STM images of the Au(111) surface a) with the mixture of undecacene precursors **22** and **23** and b) subsequently thermally generated parent **11ac** and undecaphene isomer. Tunneling current: 30 (a,b) and 150 pA (c); bias voltage: +2.0 V. c) High-resolution filled-state STM image of **11ac** with 11 lobes visible along the molecule; tunneling current: 30 pA; bias voltage: −1.0 V. Present Laplace filtered constant height, frequency-shift nc-AFM images of **11ac** (d) and its kinked isomer (e); scale bar: 5 Å. Reproduced with permission from Zuzak et al.^[58] Copyright 2018, Wiley-VCH.

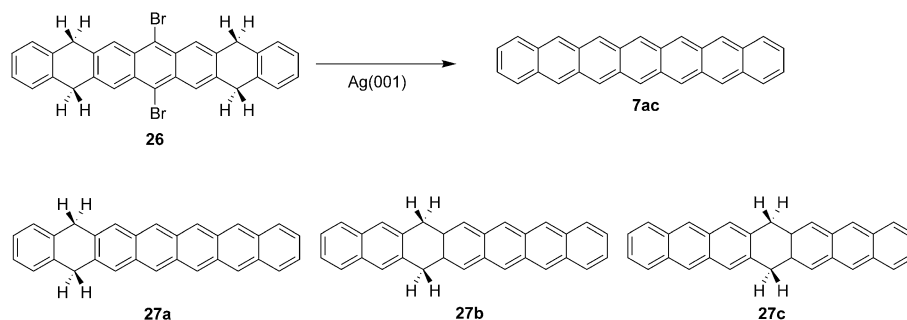
are determined to be −0.24 and 0.85 V, respectively, yielding a gap of 1.09 eV.

The dehydrogenation method was also used for the preparation of **7ac** on Ag(001) from brominated tetrahydroheptacene **26**, as well as from 5,9,14,18-tetrahydroheptacene.^[90] From both precursors, compound **7ac** is obtained through thermal dehydrogenation and the structural and electronic properties are similar. The reaction processes finally leading to **7ac** are different for the two precursors. The brominated compound is dehalogenated (at RT) and subsequent dehydrogenation is facilitated and a higher degree of aromatization is observed at 180 °C. In the partially dehydrogenated intermediates, a rearrangement of the methylene hydrogen atoms across the molecular skeleton can be observed, as shown for **27** in Scheme 9, and from different possible isomers, the one with a hydrogenated central ring, **27c**, is preferred because larger aromatic subunits destabilize the molecule. Both processes, aromatization and hydrogen migration across the molecule, are favored in the case of the brominated precursor, and this is ascribed to the initial presence of radicals after debromination. Heptacene shows a strong interaction with the Ag(001) surface, resulting in charging of the molecule.

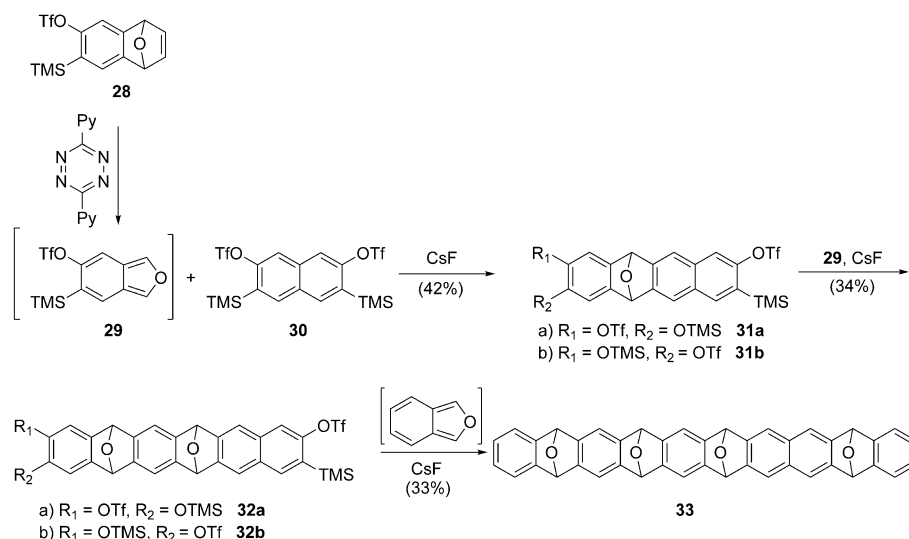
4.2. Deoxygenation of epoxyacenes

At about the same time as Zuzak et al. presented their studies on larger acenes,^[88] Krüger et al. were the first to produce **10ac**,^[91,92] following earlier on-surface generation of **6ac** on Au(111)^[93] and tetracene on Cu(111).^[94] As exemplified for the on-surface synthesis of **10ac** (Scheme 10), their precursors for acene production were epoxy derivatives that were prepared through repeated Diels–Alder reactions of arynes with isobenzofurans as an isomeric mixture of at least four of nine possible isomers of **33**.

The isomers of **33** can be sublimed under UHV onto an Au(111) surface, whereby partial deoxygenation takes place, so that mainly diepoxy precursors of **10ac** are present on the substrate. Complete deoxygenation can be achieved through annealing (220 °C) or a tip-induced procedure in a similar manner to that described above for the hydrogenated acene precursors. The planar structure of the **10ac** molecule is observed in constant-height STM measurements by using a CO-modified tip with very high resolution, revealing the structure of 10 linearly fused benzene rings. Constant-current STM measurements



Scheme 9. Formation of **7ac** on Ag(001) and observed dihydroheptacene intermediates.^[90]

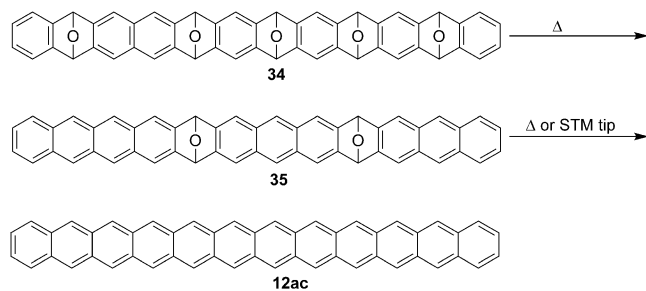


Scheme 10. Synthetic strategy for the **10ac** precursor **33**.^[91] Py = pyridyl.

after tip-assisted formation also show the planar structure of the molecules.

The STS dI/dV spectra around the Fermi level reveal six electronic resonances (called R–2, R–1, R0, R1, R2, and R3), which are ascribed to contributions from HOMO–2, HOMO–1, HOMO, LUMO, LUMO + 1, and LUMO + 2 levels, respectively, of the **10ac** molecule.^[91,92] The constant-current map of differential conductance (dI/dV) of R0 shows 10 lobes and nodal plane characteristics of the HOMO.^[91,92] Associated conductance peaks measured with a metal-terminated tip are observed at –0.32 (HOMO) and +0.85 V (LUMO), resulting in a gap of 1.17 eV. This compares well with the value of 1.12 eV determined later by Zuzak et al. for **10ac** on Au(111) produced from the hydrogenated precursor.^[58]

In 2020, Eisenhut et al. succeeded in preparing the related precursor **34** with five epoxy bridges in a sequence similar to that shown for **33** in Scheme 10.^[59] This allowed the synthesis of dodecane, the longest acene prepared so far, on an Au(111) surface (Scheme 11). During sublimation, partial deoxygenation occurs, resulting in deposition of diepoxy derivative **35** on the surface. Annealing (220 °C) causes complete deoxygenation and produces **12ac**. In addition, deoxygenation can also be



Scheme 11. Preparation of **12ac** from its pentaepoxy precursor on Au(111).^[59]

achieved through on-surface reduction of the diepoxy precursor, and it can be monitored by STM imaging, as shown in Figure 10.

Through STS, five tunneling resonances can be observed: three for negative bias voltage (R–2 to R0) and two in the positive region (R1 and R2). R0 is observed at –320 mV and R1 at 1070 mV, resulting in an energy gap of $E_g = 1.4$ eV. This value is larger than that determined for **11ac** or **10ac** and comparable in size to the value found for **8ac** (1.41 eV).^[58] This is unexpected because the STS energy gap continuously decreases in the series from pentacene to **11ac**, and the stabilization of the gap to a finite value was derived,^[92] in agreement with the analysis of the optical gap.^[56,57] The authors analyzed the energy gap more deeply and concluded that the value for R0, which is

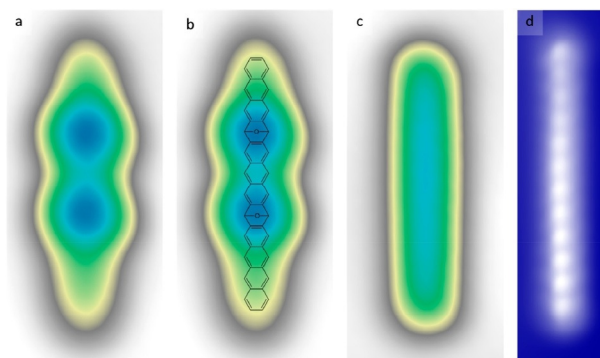


Figure 10. STM images of **12ac** on Au(111). a) STM image of **12ac** with two remaining epoxy groups. Image parameters: $V_{\text{bias}} = 2$ V, $I = 13$ pA, image size = 2 nm × 4.5 nm. b) Superposition of the STM image of a) with the structure of the partially deoxygenated precursor identifying the position of the two epoxy groups. c) STM image of a fully deoxygenated **12ac**. Image parameters: $V_{\text{bias}} = -1$ V, $I = 10$ pA, image size = 2 nm × 4.5 nm. d) Constant-height STM image obtained by using a CO-functionalized tip, recorded at $V_{\text{bias}} = 10$ mV. Twelve bright lobes, representing the 12 benzene rings, are well distinguishable. Image size: 1 nm × 4 nm. Reproduced with permission from Eisenhut et al.^[59] Copyright 2020, American Chemical Society.

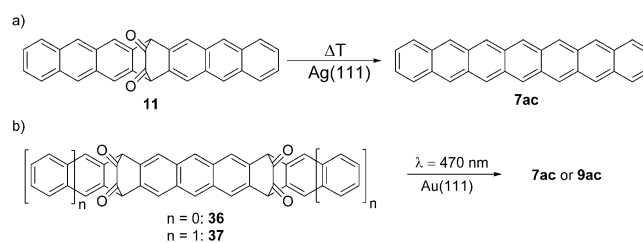
connected to the HOMO of the molecule, remained almost constant for larger acenes, whereas the energy of the R1 electronic tunneling resonance increased in the case of **12ac**.^[59] The authors considered oscillating behavior of the energy gap, as proposed by Korytár et al.^[8,95,96] based on DFT computations (see Section 5) or charge transfer to the Au surface a less likely explanation than the increase of the R1 electronic tunneling resonance energy (“destabilization”) by contributions from higher energy empty molecular orbitals.^[59] In the picture proposed by the authors, the R1 resonance of **12ac** could no longer be solely attributed to the virtual occupation of the LUMO (i.e., during the few femtoseconds of the electron-transfer event), but “involves a combination of electron transfer paths through the virtual (and instantaneous) quantum occupations of LUMO + 1, LUMO + 2, etc.”^[59]

Whereas all of the surface studies of larger acenes presented so far used gold and silver surfaces, Eisenhut et al. were able to prepare **6ac** from a triepoxy precursor on a nonmetallic hydrogen-passivated silicon surface, at which a hydrogen layer electronically decouples the molecules of **6ac** from the substrate.^[99] They could show that the epoxy precursors preferentially adsorbed at dangling-bond defects on the surface. Annealing to 250 °C did not lead to complete deoxygenation. Instead, partially deoxygenated molecules, in which the central epoxy group was removed, could be observed. Annealing to 300 °C led to the formation of **6ac**, but it was accompanied by desorption of the molecules. In contrast to the epoxy precursors studied on Au(111), voltage pulses did not lead to the generation of **6ac** on Si(001)–(2 × 1):H. The hydrogen layer spatially separated the acene by about 5 Å from the silicon surface, resulting in a small adsorption and diffusion barrier and a high mobility of the molecules on the surface, as long as they were not blocked by edges or defects. The molecules of **6ac** observed were mainly anchored to dangling-bond defects and the preferred anchoring site was on the last ring of the skeleton of **6ac**. This was visible as an apparently lower height at this site. Differential conductance spectra showed two resonances at –2.0 and –3.1 V, which were ascribed to HOMO and HOMO–1 resonances, respectively. Differential conductance measured at the position of the dangling bond site was not significantly different from that at other positions, showing that there was no strong interaction with the silicon surface. No resonances at positive bias corresponding to LUMO transitions could be observed because they were in an energy range that corresponded to the surface electronic band gap.

4.3. Decarbonylation of α -diketones

The α -diketones, which were employed in matrix isolation studies, also are precursors for the on-surface synthesis of acenes. The on-surface formation of **7ac** was investigated by Zugermeier et al. on Ag(111) by using STM, XPS, and near-edge X-ray absorption fine structure (NEXAFS) spectroscopy combined with DFT computations.^[100]

Decarbonylation was initiated by heating the deposited α -diketone precursor on Ag(111) (Scheme 12a) to about 460 K, and the reaction progress was monitored by means of XPS.



Scheme 12. On-surface generation of **7ac** and **9ac** from α -diketone precursors.^[98,100]

Based on NEXAFS data, it was concluded that molecules of **7ac** were lying with their π system on the Ag(111) surface. The STM image, however, showed that the interaction was not laterally uniform. The dumbbell shape of the molecule suggests that the interaction appears to be strongest at the central part. Such an interpretation is supported by DFT modeling of the **7ac**/Ag(111) system. The central carbon atoms C₇ and C₁₆ are closest to the Ag(111) surface (2.67 Å), whereas the terminal carbon atoms are further away (> 2.93 Å), thus resulting in a kinked structure with an angle of 3.5°. The observation was rationalized with the contribution of a diradical resonance form that featured two Clar sextets rather than one (Figure 11). A similar picture was also presented by Trinquier et al. on theoretical grounds (see below).^[101]

Acenes could also be obtained by photodecarbonylation of bis- α -diketone precursors by using visible light on metal surfaces (Scheme 12b), as shown in a recent investigation that combined STM/STS/nc-AFM for studying the formation of **7ac** and **9ac** on Au(111).^[98] In contrast to the observations on Ag(111),^[100] there was no indication of any deformation of **7ac** on Au(111). The computed molecule–Au(111) distance of 3.1 Å was interpreted as evidence for weak physisorption. Photogeneration or thermal generation of **9ac** on Au(111), in contrast, resulted in pronounced lateral protrusions close to each molecule of **9ac**. This was interpreted, with support from DFT computations, as resulting from interactions of **9ac** with two Au atoms that were “extracted”/pulled away from the surface. Again, the diradicaloid resonance form with two Clar sextets was invoked to explain the stronger interaction of central carbon atoms with the Au(111) surface. Most interestingly, the two Au adatoms can be removed by briefly applying a tunneling voltage of about 2.5 V. Pristine molecules of **9ac** result, as demonstrated by means of high-resolution STM and nc-AFM. The experimental HOMO–LUMO gaps obtained from STS experiments (see Table 1) are in good agreement with data reported by Zuzak et al.^[58,88] The good agreement between ex-

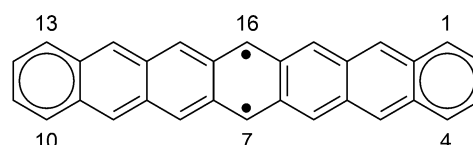


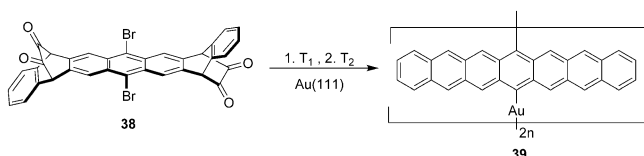
Figure 11. Diradicaloid non-Kekulé structure of **7ac**.

Table 1. A comparison of the HOMO–LUMO gaps for the acenes from pentacene to **12ac** obtained from *dI/dV* measurements and the optical gaps obtained from electronic spectra.

Acene	STS transport gap [eV]	Optical gap [eV] (λ_{max} [nm], matrix host)
pentacene	2.20 ^[97]	2.21 (562, Ar) ^[55]
hexacene	1.85 ^[93]	1.89 (655, Ar) ^[55]
heptacene	1.61 ^[58] /1.55 ^[92] /1.50 ^[98]	1.70 (728, Ar) ^[55]
octacene	1.41 ^[58]	1.53 (806, Ar) ^[56]
nonacene	1.23 ^[58] /1.19 ^[88] /1.25 ^[98]	1.43 (865, Ar) ^[56]
decacene	1.12 ^[58] /1.17 ^[91]	
undecacene	1.09 ^[58]	1.23 (1007, PS) ^[57]
dodecacene	1.4 ^[59]	

perimental *dI/dV* maps and LDOS computed for an individual molecule was considered as evidence for only weak physisorption of pristine nonacene molecules on Au(111).

The interaction with Au atoms was also observed during attempts to obtain **7ac** polymers from the dibromodiketone precursor in *anti*-orientation **38** (Scheme 13).^[102] Thermal annealing to 435 K resulted in debromination and the Au-atom-mediated interaction (C–Au (2.3 ± 0.2) Å) of bis-diketones based on the interpretation of STM images and DFT simulations. A second annealing ($T \approx 535$ K) results in decarbonylation and formation of Au-linked oligomers of **7ac**. Based on the inspection of about 900 molecules, 76% of these have lengths of 2–4 units.



Scheme 13. On-surface synthesis of **7ac**–Au complexes.^[102]

5. Theoretical Studies

There is very rich literature on theoretical studies of acenes and polyacenes that has been reviewed.^[103,104] Various properties of acenes that can, in principle, be compared with experimental data have been investigated computationally, for example, the geometric structure, IPs, EAs, singlet–triplet energy gaps, and excited-state energies. In addition, the electronic structure of the acene ground state was investigated by theory and it was tested to provide an understanding of the nature of the acene ground state.

We here start with a discussion of the singlet–triplet energy gap because its size relates to the (poly)radical character of the electronic ground state, and this property is well studied and understood for more conventional organic diradicals.^[104,105] The singlet–triplet energy difference is experimentally available for acenes up to pentacene (see Section 1).^[17] No EPR signal for **6ac** was detected up to 200 °C and the UV/Vis spectrum at 300 °C showed no indication of population of the triplet state,

providing a lower limit for the singlet–triplet gap of 6.5 kcal mol^{−1}.^[20] Correlations between the singlet–triplet gap, IPs, S_1 energies, and computed properties gave $\Delta E_{\text{ST}} \approx (12.4 \pm 1.2)$ kcal mol^{−1} as an extrapolated value for **6ac**.^[20] This value is sometimes referred to as “experimental” value in the computational literature.

Based on this extrapolation, a triplet ground state was predicted for **9ac**.^[20] The UV/Vis spectra of **8ac**, **9ac**, and **11ac** obtained experimentally under cryogenic matrix isolation conditions showed a close relationship with the smaller members of the series and no indication of population of the triplet state, and hence, the singlet state is the ground state of these larger acenes.^[56,57] The triplet ground-state nature of **9ac** appeared to be in accordance with early DFT computations that employed the spin-restricted formalism for the singlet state.^[106] However, a lower energy solution could be obtained in 2004 by Bendikov et al.,^[13] and subsequently by other groups,^[107] for the singlet state after the spin-symmetry broken (or spin-polarized) ansatz was employed, supporting the singlet nature for **9ac** and larger acenes. The spin-unrestricted DFT solution does not fulfill certain criteria of the exact wavefunction (it is not the eigenvalue of the $\langle S^2 \rangle$ operator, resulting in spin contamination, i.e., it is not a pure spin state, but a mixture, including higher spin states)^[101] and gives a nonphysical increase of ΔE_{ST} for larger acenes.^[14] The existence of a spin-contaminated, spin-unrestricted solution of the Hartree–Fock (HF)^[11,12] or Kohn–Sham (KS) equations^[13] for acenes suggests that strong nondynamic (also called static) correlation effects are present and that a single determinant description (as provided by HF and KS-DFT) of the ground state is qualitatively insufficient. Nonetheless, the singlet ground-state nature of larger acenes finds general support from studies that employ a wide variety of computational methods, including multiconfiguration treatments that are deemed more appropriate for systems with strong static correlation.^[14, 108–122]

One problem of using multiconfiguration methods for the acene series is that the active space grows quickly with the size of the system, and this makes conventional complete active space self-consistent field (CASSCF) or MRCI computations prohibitively expensive. Density matrix renormalization group (DMRG) and variational two-electron reduced density matrix (v2RDM) are methods that avoid the exponential scaling of the active space size, and thus, have been used with various quantum chemical Hamiltonians to study larger acene molecules and to extrapolate properties, such as ΔE_{ST} values, to the polymer limit, that is, to polyacene. DMRG-based MRCI computations with the Pariser–Parr–Pople (PPP) Hamiltonian estimated a singlet–triplet energy difference of 0.53 eV (12.2 kcal mol^{−1}) at the limit of polyacene.^[108] A similar value, 0.45 eV (10.1 kcal mol^{−1}), was obtained in a DMRG-based valence-bond (VB) theory study.^[113] Using the DMRG method for complete active space configuration interaction (CASCI) computations with the STO-3G and cc-pVDZ basis sets, Hachmann et al. extrapolated ΔE_{ST} values of (8.69 ± 0.95) and (3.33 ± 0.39) kcal mol^{−1}, respectively, for the polymer.^[14] The CASCI method is related to the more used CASSCF method, but lacks the orbital relaxation step of the latter. As expected, a similar singlet–trip-

let gap was obtained by v2RDM-CASSCF, which led to a value of $7.8 \text{ kcal mol}^{-1}$.^[119]

Modifications of DFT were developed that are expected to provide more robust results for systems with strong static correlation than that of conventional KS-DFT. Chai et al. introduced thermally assisted occupation (TAO) DFT, which did not suffer from spin contamination, and employed it in conjunction with local density approximation (LDA), generalized gradient approximation (GGA), and hybrid functionals for very large acenes, up to $N=100$, in a series of papers (Figure 12).^[114,115,123,124] The estimated ΔE_{ST} value of polyacene is essentially zero at the TAO-LDA/6-31G level,^[114] and 0.4 (TAO-PBE, TAO-BLYP, TAO-BLYP-D) or $0.5 \text{ kcal mol}^{-1}$ (TAO-LDA) for 100-acene (all with the 6-31G* basis set).^[115] Very similar results were obtained by using the particle-particle random-phase approximation (pp-RPA) with the B3LYP functional and cc-pVDZ basis set.^[116] The value estimated for ΔE_{ST} in the limit of infinitely long polyacene is between 0.0 and 0.1 eV ($2.3 \text{ kcal mol}^{-1}$).^[116] Multiconfiguration pair density functional theory (PDFT) based on v2RDM-CASSCF arrives at ΔE_{ST} values of 4.8–4.9 kcal mol^{-1} with on-top PDFT versions (“translated”) of the PBE and BLYP functionals extrapolated from data up to **12ac**.^[120]

The gold standard of quantum chemistry, coupled cluster theory with single, double, and a perturbative estimate of triple excitations, CCSD(T), was employed for longer acenes. The use of focal point analyses allowed the estimation of CCSD(T) data in the limit of infinitely large basis sets, cc-pV ∞ Z.^[110,111] The CCSD(T)/cc-pV ∞ Z computations, up to **7ac** and subsequently extended to **11ac**, led to the conclusion that the singlet–triplet energy gap vanished in the polymer limit with an uncertainty of $1.5 \text{ kcal mol}^{-1}$.^[110,111] One problem of the CCSD(T) method is that it is based on a single HF determinant and, in cases of strong nondynamic correlation, the performance of the CCSD(T) may be poorer than usual. There are diagnostics available to allow the appropriateness of the single HF determinant to be determined. The T_1 diagnostic for acenes up to **11ac** (0.0117) is much smaller than the critical value of

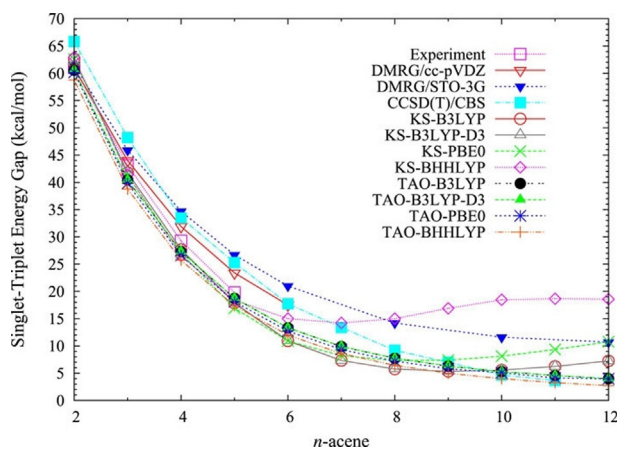


Figure 12. Singlet–triplet energy gaps as a function of the acene length, calculated using various hybrid functionals in spin-unrestricted KS-DFT and TAO-DFT according to Chai et al.^[123] Copyright 2017, AIP Publishing.

0.02. Plasser et al., however, pointed out that the D_2 diagnostic associated with double excitations of the sort relevant for acenes was larger than that of the recommended threshold.^[115] In addition, Lee et al. showed that the RCCSD methods behaved unreliably, even for smaller acenes.^[125] This suggests that the CCSD(T) data should be considered with more caution than usual.

The spin-flip (SF) approach allows treating static correlation, and in combination with methods that take into account dynamic correlation (e.g., DFT, MP2, CCSD), both types of correlation can, in principle, be described in a balanced manner. From data computed at the SF-CCSD/6-31G* level for acenes up to **6ac**, a ΔE_{ST} value in the limit of an infinitely long polyacene of $5.4 \text{ kcal mol}^{-1}$ was extrapolated.^[117] This value is reduced to $5.1 \text{ kcal mol}^{-1}$ after applying method and basis set corrections.^[117]

To summarize, almost all computational methods (an exception is fractional-spin DFT^[126]) applied to acenes agreed that the singlet remains the ground state and the singlet–triplet energy gap approached a small value for an infinitely long polyacene. The methods agree that, for the currently largest experimentally accessible acenes, **11ac** and **12ac**, the singlet–triplet energy splitting is 3–5 kcal mol^{-1} (Table 2). Compared with more traditional organic diradicals, such a gap is similar to that of *p*-benzyne ($(3.8 \pm 0.4) \text{ kcal mol}^{-1}$),^[18] a highly reactive 1,4-diradical.^[127,128]

An important aspect of any sophisticated quantum chemical treatment is the geometrical structure that is employed. Many of the methods mentioned in this section do not allow geometry optimization because their first derivatives of the wavefunction, with respect to coordinates, have not been implemented or are computationally too demanding if performed by numerical differentiation. Thus, it is common practice to resort to some density functional for geometry optimization and limit the sophisticated correlation treatment to subsequent energy refinement. However, apart from these technical aspects, the geometry of acenes are of fundamental interest, as well. Because it was predicted that, with increasing size of the system, polyacene in its high-symmetry configuration (i.e., without bond-length alternation (BLA)) might become an organic semi-metallic conductor with a vanishing band gap, the quasi-one-

Table 2. Computed adiabatic singlet–triplet energy splittings (in kcal mol^{-1}) of experimentally accessible acenes.

<i>N</i>	pp-RPA-B3LYP/ cc-pVDZ ^[116]	TAO-PBE/ 6-31G* ^[115]	TAO-B3LYP/ 6-31G* ^[123]	CCSD(T)/ cc-pV ∞ Z ^[111]	Exptl
5	22.6	17.6	18.7	23.9	19.8 ± 0.7 ^[17]
6	16.4	11.8	13.3	16.5	12.4 ± 1.2 ^[a]
7	11.8	n.a. ^[b]	9.9	12.3	n.a. ^[b]
8	8.5	6.4	7.7	8.2	n.a. ^[b]
9	6.5	n.a. ^[b]	6.3	6.1	n.a. ^[b]
10	5.1	4.7	5.3	3.7	n.a. ^[b]
11	4.2	n.a. ^[b]	4.6	2.6	n.a. ^[b]
12	3.7	3.8	4.0	n.a.	n.a. ^[b]

[a] Estimated value; see Angliker et al. for details.^[20] [b] n.a. = not available.

dimensional system could gain energy by undergoing a geometrical distortion and thereby create a band gap.^[6,7,129,130] Early studies focused on the possibility of a Peierls- or Jahn-Teller distortion of the polyacene structural framework and found that there was no “intrinsic instability in the symmetrical equilibrium configuration,”^[6] because, due to symmetry considerations of the relevant crystal orbitals, no driving force for the geometrical distortion exists.^[6] Although other views have been expressed, as reviewed earlier,^[103] recent TAO-LDA computations concur with this conclusion and give a symmetrical structure for 46-acene.^[114] The 20 inner rings have equal bond lengths of 1.399 Å. The two terminal rings have BLA of 0.046 Å, which successively decreases upon approaching the inner rings.^[114] The lengths of the ring bonds increase from 1.42 Å in the terminal ring (C2–C3 bond) to 1.45 in the inside of the molecule.^[114] These computations show that, even for very large acenes, the symmetric configuration without BLA is favored.

Another related property of interest is the optical gap of the acenes, that is, the energy difference between the electronic ground state and the first electronically excited singlet state, to which the transition is electric dipole allowed within the Franck–Condon approximation. For acenes up to **11ac**, the optical spectra were recorded by using matrix isolation spectroscopy (see above), and the transition energy to the first excited state that was electric dipole allowed within the Franck–Condon approximation could be obtained. This state is very strongly dominated by an excitation of a single electron from HOMO to LUMO, that is, $H \rightarrow L$ (1^1B_{2u}).^[80] For acenes up to **11ac**, sophisticated DFT/MRCI computations were also performed that concurred with the nature of this excitation.^[81] Notably, however, according to these computations, there are weakly absorbing excited states that are lower in energy than that of the bright $H \rightarrow L$ excited state and that are related to excitation of two electrons, that is, $H-1, H \rightarrow L, L$ and $H, H \rightarrow L, L+1$ (1^1B_{3u}).^[81] These states have not been observed in the experiments, presumably due to their very low oscillator strengths.^[56,57] The energy gap involving the $H \rightarrow L$ (1^1B_{2u}) electronic transition was estimated to converge to 1.23 eV based on available experimental data.^[56,57] The energy of the 1^1B_{2u} state was also investigated by using pp-RPA-B3LYP/cc-pVDZ up to **12ac**.^[116] It appears that the method underestimates the energies of this state by about 0.2 eV, by comparison with experiment and DFT/MRCI. An extrapolation of the pp-RPA-B3LYP data to the polyacene limit arrives at an optical gap of 0.85 eV.^[116] A larger optical gap of 1.21 eV for polyacene was obtained by extrapolation for values up to **10ac** computed with the excited-spectra two-electron reduced density matrix (ES-RDM) method.^[131]

In addition to the singlet–triplet energy gap and singlet–singlet optical gap, the fundamental gap, that is, the difference between the IP and EA, $E_g = IP - EA$, were evaluated computationally for the acene series. The gas-phase experimental EAs are available up to pentacene (Table 3),^[19] whereas IPs have been determined experimentally up to **6ac** (Table 4).^[132] The most sophisticated computational evaluation of the IP and EA values was performed by using focal-point analysis and provided data at the CCSD(T)/cc-pV ∞ Z level up to **6ac**.^[133,134] In addition,

Table 3. A comparison of computed vertical and adiabatic EAs (vEA and aEA, respectively) with experimental data (in eV).

<i>N</i>	vEA CCSD(T) ^[134]	aEA CCSD(T) ^[134]	vEA TAO-PBE ^[115]	vEA TAO-B3LYP ^[123]	Exptl ^[132]
3	0.28	0.52	0.16	0.04	0.57
4	0.82	1.02	0.77	0.64	1.04 ± 0.04
5	1.21	1.39	1.20	1.07	1.35 ± 0.04
6	1.47	1.63	1.52	1.38	n.a.

Table 4. A comparison of computed vertical and adiabatic IPs (vIP and aIP, respectively) with experimental data (in eV).

<i>N</i>	vIP CCSD(T) ^[133]	aIP CCSD(T) ^[133]	vIP TAO-PBE ^[115]	vIP TAO-B3LYP ^[123]	Exptl ^[19]
3	7.47(3)	7.41(9)	6.79	6.74	7.41
4	6.94(8)	6.91(4)	6.25	6.20	6.97
5	6.57(3)	6.55(6)	5.87	5.82	6.61
6	6.43	6.42	5.59	5.55	6.36

tion, vertical EA and IP values were also obtained at the TAO-DFT level for acenes up to 100 rings.^[115,123] It is seen by comparison with experimental values that the TAO-DFT methods underestimate the IP significantly (Table 4). The fundamental gap obtained for 100-acene with TAO-PBE (and other functionals) is around 0.55 eV,^[115] suggesting that a nonzero fundamental gap is expected for very large acenes. The fundamental gap was found to decrease monotonically by using the TAO-B3LYP/6-31G* method up to $N=30$, which was the largest acene that was investigated.^[123] Its fundamental gap is 1.36 eV at this level of theory.^[123]

Closely related to the fundamental gap, $E_g = IP - EA$, is the HOMO–LUMO energy gap, which was derived from single reference computations employing, for example, the Hubbard model or KS-DFT.^[8,95,96] It was concluded that the orbital energy gap of the oligoacenes did not decrease monotonously with increasing length, but oscillated and could become zero or nearly zero at so-called Dirac points of the band structure.^[8,95,96] The oscillations are called incommensurate oscillations (IOs) because the oscillation period is not dictated by the lattice symmetry and the period can be 10 times the length of a unit cell. The reason for this is the change of the symmetry of HOMO and LUMO close to **10ac**. The computations did not take into account static correlation, which is undoubtedly of high importance in this length regime. Indeed, eigenvalue-self-consistent GW (evGW) computations of the HOMO–LUMO gap only give a gap increase if an (inappropriate) spin-restricted (“closed-shell”) DFT (PBE0 and tuned CAM-B3LYP functionals) description is employed and restore the monotonic decrease if spin-symmetry broken (“open-shell”) DFT is used.^[135] Moresco et al. have shown that inclusion of doubly excited Slater determinants ($H, H \rightarrow L, L$) in a simple Hückel–Hubbard model eliminates the band gap oscillation,^[92] in agreement with measurements of the experimental tunneling electronic gap between the frontier resonances up to **10ac**^[92] and **11ac**^[58] on Au(111). These authors have thus concluded that the gap increase that

they have observed for **12ac** on Au(111) is not associated with the band gap oscillation, but rather with the polyradical character of the singlet ground state (see Section 4.2).^[59]

What is the nature of the ground state of acenes? The finding of the lower energy spin-symmetry-broken KS-DFT solution by Bendikov et al. suggested an “open-shell singlet diradical ground state” from **7ac** on.^[13] Notably, such a species would not be EPR active because the overall spin multiplicity is singlet. Indeed, compound **7ac** is EPR silent.^[54] The DMRG-based CAS-CI study of Hachmann et al. analyzed the singlet ground state of larger acenes by using natural orbitals and correlation functions for its description.^[14] Based on the natural orbital occupation numbers (NOONs), which more strongly deviate from the values zero and two expected for closed-shell systems with increasing acene length, these authors concluded that the ground states of large acenes should eventually acquire “polyradical” character.^[14] In this picture, an antiferromagnetic ground state of the acene molecules evolves.^[14] Similar deviations of NOONs were observed in a number of other studies with related approaches (v2RDM-based CAS),^[121,136–139] and different Hamiltonians, including MR-AQCC,^[15] TAO-DFT,^[114,115] and pp-RPA-B3LYP.^[116]

The amount of polyradical nature for a given acene length, however, depends on the level of theory. Although Hachmann et al., referring to their Figure 5, cautioned that the “values should not be taken literally,”^[14] Hajgató et al. argued, in their focal-point analysis, at the coupled-cluster level that the degree of (poly)radical nature was overestimated for smaller acenes.^[110] However, Lee et al. have shown that the NOONs of RCCSD,^[125] presumed to describe a closed-shell ground state,^[110,111] suggest a *larger* diradical character than that derived from DMRG-CASCI. Hajgató et al. forcefully opposed the antiferromagnetically ordered ground states as arising from artifactual symmetry breaking due to methodological deficiencies and argued, based on weights of the CASSCF wavefunction, size of the coupled-cluster T_1 diagnostic, comparison of MP2 and CASPT2 singlet–triplet gaps, and percentages of total atomization energies at RHF and connected triples, that the smaller acenes were closed-shell systems.^[110] They have no particularly strong nondynamic correlation in their view, but are dominated by dynamic correlation that should be recovered by CCSD(T).^[110] However, the D_2 diagnostic is already above the threshold (0.18) for naphthalene (0.203) and increases quickly up to **8ac** (0.253),^[15] and that RCCSD behaves nonvariationally for naphthalene.^[125]

Yang et al. looked at the multireference character by using the dominant configuration contribution (DCC) as its measure obtained from the pp-RPA-B3LYP computations.^[116] They concluded that acenes up to **10ac** could be described as closed-shell systems and, at a larger size, an open-shell treatment was necessary as the polyradical character started to emerge.^[116] Analysis of the SF-CCSD wavefunctions suggested that anthracene only had a small amount of diradical character, whereas for **10ac** a “significant” amount of di- and tetradical character emerged.^[117] The DFT/MRCI computations that included a full-valence π space showed that the doubly excited configuration $H^2 \rightarrow L^2$ contributed to the wavefunction of heptacene with

10%, but this weight increased to 16% (**8ac**), 23% (**9ac**), 25% (**10ac**), and 29% (**11ac**).^[57,81] The importance of double excitation for the appearance of spin instability was discussed by Trinquier et al.^[101] As the weight of the double excitation increases, the weight of the closed-shell reference decreases from 74% to 29% from **8ac** to **11ac**, respectively.^[57,81] Various studies, for example, coupled-cluster VB singles and doubles (CCVB-SD), ACI-DSRG-MRPT2, show that the π -space (poly)radical character is reduced upon inclusion of σ -electron correlation and increase of the basis set,^[125,140,141] but that short-range antiferromagnetic order is preserved.^[141]

The crossover of closed- to open-shell singlet (CSS and OSS) nature of the electronic ground state was also investigated by using quantum Monte Carlo (QMC) and the Jastrow single and double determinant (JSD and JDD, respectively), as well as the Jastrow antisymmetric geminal power (JAGP) wavefunctions.^[118] JSD only includes dynamic correlation and is thus deemed to represent CSS state similar to coupled-cluster theory.^[118] It should be remembered that a large diradical character was shown for the RCCSD wavefunction based on the NOON.^[125] JDD, on the other hand, explicitly includes HOMO–LUMO excitations, whereas JAGP is the wavefunction representation of the resonating valence-bond (RVB) theory.^[118] The JSD results closely reproduce the earlier CCSD(T) data,^[110,111] but JDD and, even more so, JAGP, absolute energies are lower.^[118] Based on the variational principle, the JAGP wavefunction represents the ground state best. Because its properties are more similar to the JSD than the JDD results, the degree of OSS nature of the systems predicted by JDD is considered an overestimation.^[118] A comparison of occupation numbers of highest occupied and lowest unoccupied orbitals (HONO and LUNO, respectively), spin–spin correlation functions, geometries, and aromaticity indices suggest that there is a “non-negligible antiferromagnetic correlation,” and a “highly correlated multireference GS, where however the diradical character is significantly weakened, although always present in this class of systems for large enough sizes” upon going from the JDD to JAGP description.^[118] It was concluded that the diradical character up to **9ac** was weak and slowly increased with acene length.^[118]

A qualitative pictorial description of the polyradical character of acenes was developed by Trinquier et al. based on a spin-symmetry-broken B3LYP analysis.^[101,142] Similar to the non-Kekulé structure invoked by Zugermeier et al. for **7ac**/Ag(111) (see Figure 11),^[100] the authors increased the number of Clar sextets and introduced two delocalized radicals along the two chains of the acene that extended roughly over five rings for **7ac** and corresponding tetradicals and so on for larger acenes (Figure 13).^[101] Even if the diradical character is weakened, as suggested by the QMC-JAGP study,^[118] the qualitative picture of Trinquier et al. prevails.^[101,142] The onset of the diradicaloid structure is then shifted to longer acenes than that of **7ac**.

Another qualitative picture based on Clar sextets was provided by Bhattacharya et al.^[4] These authors stressed the similarity of the Clar sextet with resonance theory because Clar’s sextet can be considered to include two Kekulé and three “Dewar” resonance structures, the latter with very little weight

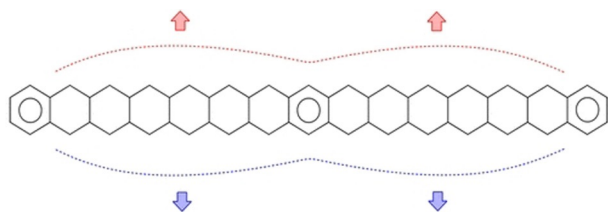


Figure 13. Pictorial representation of the tetraradical character in pentadecacene ($N=15$), according to Trinquier et al.^[101] Copyright 2018, American Chemical Society.

(Figure 14a). Considering next-next-nearest neighbor sites “outside” a Clar sextet, as introduced by configuration interaction, gives rise to many “extended” Clar sextet structures. One of these has an additional Clar sextet (see the boxed resonance form in Figure 14b for anthracene). Its contribution is deemed unimportant for anthracene, but the importance of double-sextet structures increases quickly with acene size because more and more of them can be generated. Neglecting the nonvertical resonance forms that destroy Clar sextets, for tetracene, four double-sextet structures are available.

Allowing multiple long bonds, with less weight, provides a way to increase the number of Clar sextets further, for exam-

ple, to triple sextet structures of pentacene and **6ac** (Figure 14c). Because a long bond is weak and easier to break and replace by a triplet spin-pairing or an antiferromagnetic arrangement without decreasing the number of Clar sextets, the triplet or OSS state is stabilized and the electronic structure develops towards (poly)radical character.^[4]

6. Summary and Outlook

Research efforts in a number of laboratories, experimental and computational alike, have led to a significant increase in the understanding of acenes during the last decade. The optical and tunneling electronic gap between the frontier resonances were determined for systems as large as **11ac** and **12ac**, respectively. Computational investigations provided deep insight into the electronic structure of the ground state and some of the electronically excited states.

However, many fundamental properties are still elusive for systems larger than that of **6ac**, such as the IPs and EAs, the sizes of the singlet–triplet energy gaps, the further evolution of the optical properties and gaps, or the stability and reactivity under “conventional” organic chemistry conditions. It is not even clear if acenes larger than that of **7ac** can exist outside the special environment provided by matrix isolation or on-sur-

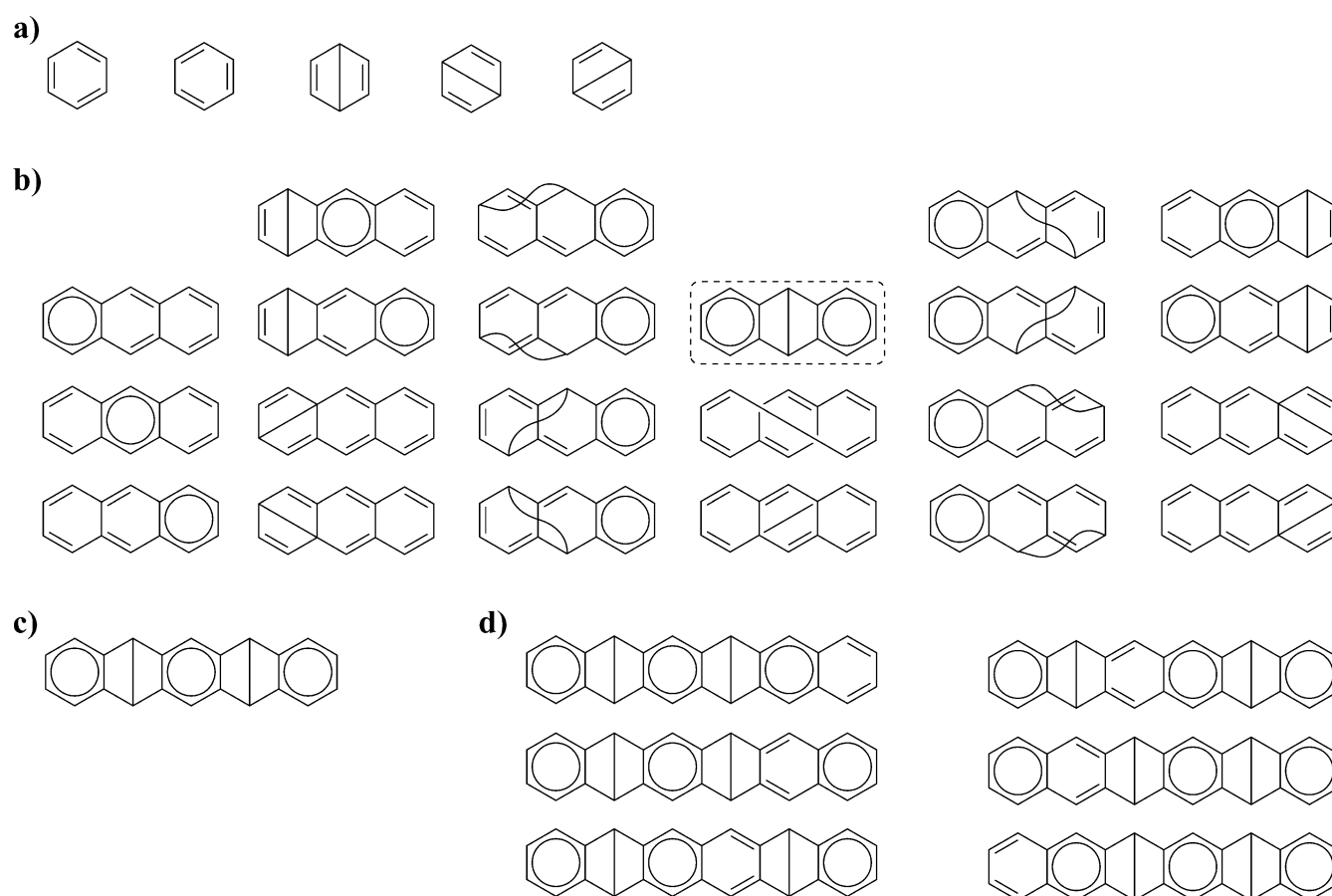


Figure 14. a) Resonance structures of benzene that are represented within the Clar sextet. b) Extended Clar sextet structures with no more than a single bond for anthracene. c) Double long-bond structures admitting three Clar sextets for pentacene. d) Double long-bond structures admitting three Clar sextets for **6ac**. Adapted from Bhattacharya et al.^[4]

face synthesis. Indeed, recent success by on-surface synthetic and associated analytical methods is currently limited to sub-monolayer coverage and important questions are unanswered: what happens to the molecules beyond the monolayer? Can molecular films, which are required for applications such as OFETs or LEDs, be grown? Can long acenes be employed for charge transport along the long molecular axis? Despite recent progress, there is much more work to do to fully understand this fascinating and unique class of organic π systems.

Note added in Proof: Very recently heptacene could be photogenerated from its dicarbonyl precursor within a single crystal inside the protective environment of its precursor.^[143]

Acknowledgements

We thank the Deutsche Forschungsgemeinschaft for financial support of the fundamental research on parent acenes in Tübingen. We thank Dr. Peter Grüninger for comments on the manuscript. H.F.B. thanks Prof. Dr. Douglas C. Neckers for the fruitful cooperation that initiated acene research in the Bettinger research group. Open access funding enabled and organized by Projekt DEAL.

Conflict of interest

The authors declare no conflict of interest.

Keywords: acenes • density functional calculations • fused-ring systems • polycyclic aromatic hydrocarbons • surface chemistry

- [1] G. P. Moss, P. A. S. Smith, D. Tavernier, *Pure Appl. Chem.* **1995**, *67*, 1307.
- [2] E. Clar, *The Aromatic Sextet*, Wiley-Interscience, London, **1972**.
- [3] M. Solà, *Front. Chem.* **2013**, *1*, 22.
- [4] D. Bhattacharya, A. Panda, A. Misra, D. J. Klein, *J. Phys. Chem. A* **2014**, *118*, 4325.
- [5] A. Misra, D. J. Klein, T. Morikawa, *J. Phys. Chem. A* **2009**, *113*, 1151.
- [6] L. Salem, H. C. Longuet-Higgins, *Proc. R. Soc. London Ser. A* **1960**, *255*, 435.
- [7] S. Kivelson, O. L. Chapman, *Phys. Rev. B* **1983**, *28*, 7236.
- [8] R. Korytár, D. Xenioti, P. Schmitteckert, M. Alouani, F. Evers, *Nat. Commun.* **2014**, *5*, 5000.
- [9] M. Baldo, G. Piccitto, R. Pucci, P. Tomasello, *Phys. Lett.* **1983**, *95A*, 201.
- [10] M. Kimura, H. Kawabe, K. Nishikawa, S. Aono, *J. Chem. Phys.* **1986**, *85*, 3090.
- [11] M. Baldo, A. Grassi, R. Pucci, P. Tomasello, *J. Chem. Phys.* **1982**, *77*, 2438.
- [12] D. Dehareng, G. Dive, *J. Comput. Chem.* **2000**, *21*, 483.
- [13] M. Bendikov, H. M. Duong, K. Starkey, K. N. Houk, E. A. Carter, F. Wudl, *J. Am. Chem. Soc.* **2004**, *126*, 7416.
- [14] J. Hachmann, J. J. Dorando, M. Avilés, G. K.-L. Chan, *J. Chem. Phys.* **2007**, *127*, 134309.
- [15] F. Plasser, H. Pašalić, M. H. Gerzabek, F. Libisch, R. Reiter, J. Burgdörfer, T. Müller, R. Shepard, H. Lischka, *Angew. Chem. Int. Ed.* **2013**, *52*, 2581; *Angew. Chem.* **2013**, *125*, 2641.
- [16] P. Rivero, C. A. Jiménez-Hoyos, G. E. Scuseria, *J. Phys. Chem. B* **2013**, *117*, 12750.
- [17] J. Burgos, M. Pope, C. E. Swenberg, R. R. Alfano, *Phys. Status Solidi B* **1977**, *83*, 249.
- [18] P. G. Wenthold, R. R. Squires, W. C. Lineberger, *J. Am. Chem. Soc.* **1998**, *120*, 5279.
- [19] D. Biermann, W. Schmidt, *J. Am. Chem. Soc.* **1980**, *102*, 3163.
- [20] H. Angliker, E. Rommel, J. Wirz, *Chem. Phys. Lett.* **1982**, *87*, 208.
- [21] N. Nijgorodov, V. Ramachandran, D. P. Winkoun, *Spectrochim. Acta Part A* **1997**, *53*, 1813.
- [22] M. Bendikov, F. Wudl, D. F. Perepichka, *Chem. Rev.* **2004**, *104*, 4891.
- [23] J. E. Anthony, *Chem. Rev.* **2006**, *106*, 5028.
- [24] J. E. Anthony, *Angew. Chem. Int. Ed.* **2008**, *47*, 452; *Angew. Chem.* **2008**, *120*, 460.
- [25] K. J. Thorley, J. E. Anthony, *Isr. J. Chem.* **2014**, *54*, 642.
- [26] F. Ortman, K. S. Radke, A. Günther, D. Kasemann, K. Leo, G. Cuniberti, *Adv. Funct. Mater.* **2015**, *25*, 1933.
- [27] N. V. Korovina, N. F. Pompetti, J. C. Johnson, *J. Chem. Phys.* **2020**, *152*, 040904.
- [28] C. Hetzer, D. M. Guldi, R. R. Tykwinski, *Chem. Eur. J.* **2018**, *24*, 8245.
- [29] R. R. Tykwinski, *Acc. Chem. Res.* **2019**, *52*, 2056.
- [30] S. S. Zade, N. Zamoshchik, A. R. Reddy, G. Fridman-Marueli, D. Sheberla, M. Bendikov, *J. Am. Chem. Soc.* **2011**, *133*, 10803.
- [31] N. Zamoshchik, S. S. Zade, M. Bendikov, *J. Org. Chem.* **2013**, *78*, 10058.
- [32] W. Fudickar, T. Linker, *J. Am. Chem. Soc.* **2012**, *134*, 15071.
- [33] R. Mondal, R. M. Adhikari, B. K. Shah, D. C. Neckers, *Org. Lett.* **2007**, *9*, 2505.
- [34] E. Clar, *Ber. Dtsch. Chem. Ges.* **1939**, *72B*, 1817.
- [35] C. Marschalk, *Bull. Soc. Chim. Fr.* **1939**, *6*, 1112.
- [36] E. Clar, *Ber. Dtsch. Chem. Ges. B* **1942**, *75B*, 1283.
- [37] W. J. Bailey, C.-W. Liao, *J. Am. Chem. Soc.* **1955**, *77*, 992.
- [38] K. F. Lang, M. Zander, *Chem. Ber.* **1963**, *96*, 707.
- [39] M. P. Satchell, B. E. Stacey, *J. Chem. Soc. C* **1971**, 468.
- [40] M. Watanabe, Y. J. Chang, S.-W. Liu, T.-H. Chao, K. Goto, M. Minaril-Islam, C.-H. Yuan, Y.-T. Tao, T. Shinmyozu, T. J. Chow, *Nat. Chem.* **2012**, *4*, 574.
- [41] R. B. Campbell, J. M. Robertson, J. Trotter, *Acta Crystallogr.* **1962**, *15*, 289.
- [42] J. Preuss, V. Zanker, *Z. Naturforsch. A* **1974**, *29*, 352.
- [43] E. Busby, T. C. Berkelbach, B. Kumar, A. Chernikov, Y. Zhong, H. Hlaing, X. Y. Zhu, T. F. Heinz, M. S. Hybertsen, M. Y. Sfeir, D. R. Reichman, C. Nuckolls, O. Yaffe, *J. Am. Chem. Soc.* **2014**, *136*, 10654.
- [44] G. P. Miller, J. Mack, J. Briggs, *Org. Lett.* **2000**, *2*, 3983.
- [45] J. E. Anthony, J. S. Brooks, D. L. Eaton, S. R. Parkin, *J. Am. Chem. Soc.* **2001**, *123*, 9482.
- [46] M. M. Payne, S. R. Parkin, J. E. Anthony, *J. Am. Chem. Soc.* **2005**, *127*, 8028.
- [47] B. Purushothaman, S. R. Parkin, J. E. Anthony, *Org. Lett.* **2010**, *12*, 2060.
- [48] D. Chun, Y. Cheng, F. Wudl, *Angew. Chem. Int. Ed.* **2008**, *47*, 8380; *Angew. Chem.* **2008**, *120*, 8508.
- [49] I. Kaur, N. N. Stein, R. P. Koperski, G. P. Miller, *J. Am. Chem. Soc.* **2009**, *131*, 3424.
- [50] H. Qu, C. Chi, *Org. Lett.* **2010**, *12*, 3360.
- [51] I. Kaur, M. Jazdzzyk, N. N. Stein, P. Prusevich, G. P. Miller, *J. Am. Chem. Soc.* **2010**, *132*, 1261.
- [52] B. Purushothaman, M. Bruzek, S. R. Parkin, A.-F. Miller, J. E. Anthony, *Angew. Chem. Int. Ed.* **2011**, *50*, 7013; *Angew. Chem.* **2011**, *123*, 7151.
- [53] R. Mondal, B. K. Shah, D. C. Neckers, *J. Am. Chem. Soc.* **2006**, *128*, 9612.
- [54] H. F. Bettinger, R. Mondal, D. C. Neckers, *Chem. Commun.* **2007**, 5209.
- [55] R. Mondal, C. Tönshoff, D. Khon, D. C. Neckers, H. F. Bettinger, *J. Am. Chem. Soc.* **2009**, *131*, 14281.
- [56] C. Tönshoff, H. F. Bettinger, *Angew. Chem. Int. Ed.* **2010**, *49*, 4125; *Angew. Chem.* **2010**, *122*, 4219.
- [57] B. Shen, J. Tatchen, E. Sanchez-García, H. F. Bettinger, *Angew. Chem. Int. Ed.* **2018**, *57*, 10506; *Angew. Chem.* **2018**, *130*, 10666.
- [58] R. Zuzak, R. Dorel, M. Kolmer, M. Szymanski, S. Godlewski, A. M. Echavarren, *Angew. Chem. Int. Ed.* **2018**, *57*, 10500; *Angew. Chem.* **2018**, *130*, 10660.
- [59] F. Eisenhut, T. Kühne, F. García, S. Fernández, E. Guitián, D. Pérez, G. Trinquier, G. Cuniberti, C. Joachim, D. Peña, F. Moresco, *ACS Nano* **2020**, *14*, 1011.
- [60] C. Tönshoff, H. F. Bettinger, *Top. Curr. Chem.* **2014**, *349*, 1.
- [61] H. F. Bettinger, C. Tönshoff, *Chem. Rec.* **2015**, *15*, 364.
- [62] M. Watanabe, K.-Y. Chen, Y. J. Chang, T. J. Chow, *Acc. Chem. Res.* **2013**, *46*, 1606.
- [63] M. Watanabe, W.-T. Su, K.-Y. Chen, C.-T. Chien, T.-H. Chao, Y. J. Chang, S.-W. Liu, T. J. Chow, *Chem. Commun.* **2013**, *49*, 2240.

- [64] M. Watanabe, T. Miyazaki, T. Matsushima, J. Matsuda, C.-T. Chein, M. Shibahara, C. Adachi, S.-S. Sun, T. J. Chow, T. Ishihara, *RSC Adv.* **2018**, *8*, 13259.
- [65] J. Han, X. Liu, Y. Li, Z. Lou, M. Yi, H. Kong, J. Luo, *Org. Chem. Front.* **2019**, *6*, 2839.
- [66] P. Grüninger, M. Polek, M. Ivanovic, D. Balle, R. Karstens, P. Nagel, M. Merz, S. Schuppler, R. Ovsyannikov, H. F. Bettinger, H. Peisert, T. Chassé, *J. Phys. Chem. C* **2018**, *122*, 19491.
- [67] P. Grüninger, K. Greulich, R. Karstens, A. Belsler, R. Ovsyannikov, E. Giangristostomi, H. F. Bettinger, D. Batchelor, H. Peisert, T. Chassé, *J. Phys. Chem. C* **2019**, *123*, 27672.
- [68] E. Clar, *Ber. Dtsch. Chem. Ges.* **1942**, *75B*, 1330.
- [69] R. Einholz, T. Fang, R. Berger, P. Grüninger, A. Früh, T. Chassé, R. F. Fink, H. F. Bettinger, *J. Am. Chem. Soc.* **2017**, *139*, 4435.
- [70] A. Jancarik, G. Levet, A. Gourdon, *Chem. Eur. J.* **2019**, *25*, 2366.
- [71] T. Fang, Ph. D. Thesis, University of California, Los Angeles (Los Angeles, CA, USA), **1986**.
- [72] J. Strating, B. Zwanenburg, A. Wagenaar, A. C. Udding, *Tetrahedron Lett.* **1969**, *10*, 125.
- [73] R. Mondal, A. N. Okhrimenko, B. K. Shah, D. C. Neckers, *J. Phys. Chem. B* **2008**, *112*, 11.
- [74] H. F. Bettinger, R. Mondal, M. Krasowska, D. C. Neckers, *J. Org. Chem.* **2013**, *78*, 1851.
- [75] M. B. Rubin, A. Patyk, W. Sander, *Tetrahedron Lett.* **1988**, *29*, 6641.
- [76] R. Mondal, B. K. Shah, D. C. Neckers, *J. Photochem. Photobiol. A* **2007**, *192*, 36.
- [77] H. Uno, Y. Yamashita, M. Kikuchi, H. Watanabe, H. Yamada, T. Okujima, T. Ogawa, N. Ono, *Tetrahedron Lett.* **2005**, *46*, 1981.
- [78] H. Yamada, Y. Yamashita, M. Kikuchi, H. Watanabe, T. Okujima, H. Uno, T. Ogawa, K. Ohara, N. Ono, *Chem. Eur. J.* **2005**, *11*, 6212.
- [79] M. Suzuki, T. Aotake, Y. Yamaguchi, N. Noguchi, H. Nakano, K.-i. Nakayama, H. Yamada, *J. Photochem. Photobiol. C* **2014**, *18*, 50.
- [80] M. Klessinger, J. Michl, *Excited States and Photochemistry of Organic Molecules*, VCH Publishers, New York, **1989**.
- [81] H. F. Bettinger, C. Tönshoff, M. Doerr, E. Sanchez-García, *J. Chem. Theory Comput.* **2016**, *12*, 305.
- [82] L. Gross, B. Schuler, N. Pavliček, S. Fatayer, Z. Majzik, N. Moll, D. Peña, G. Meyer, *Angew. Chem. Int. Ed.* **2018**, *57*, 3888; *Angew. Chem.* **2018**, *130*, 3950.
- [83] I. Swart, L. Gross, P. Liljeroth, *Chem. Commun.* **2011**, *47*, 9011.
- [84] D. M. Eigler, C. P. Lutz, W. E. Rudge, *Nature* **1991**, *352*, 600.
- [85] L. Bartels, G. Meyer, K. H. Rieder, *Appl. Phys. Lett.* **1997**, *71*, 213.
- [86] L. Gross, F. Mohn, N. Moll, P. Liljeroth, G. Meyer, *Science* **2009**, *325*, 1110.
- [87] S. Clair, D. G. de Oteyza, *Chem. Rev.* **2019**, *119*, 4717.
- [88] R. Zuzak, R. Dorel, M. Krawiec, B. Such, M. Kolmer, M. Szymanski, A. M. Echavarren, S. Godlewski, *ACS Nano* **2017**, *11*, 9321.
- [89] R. Dorel, P. R. McGonigal, A. M. Echavarren, *Angew. Chem. Int. Ed.* **2016**, *55*, 11120; *Angew. Chem.* **2016**, *128*, 11286.
- [90] L. Colazzo, M. S. G. Mohammed, R. Dorel, P. Nita, C. García Fernández, P. Abufager, N. Lorente, A. M. Echavarren, D. G. de Oteyza, *Chem. Commun.* **2018**, *54*, 10260.
- [91] J. Krüger, F. García, F. Eisenhut, D. Skidin, J. M. Alonso, E. Guitián, D. Pérez, G. Cuniberti, F. Moresco, D. Peña, *Angew. Chem. Int. Ed.* **2017**, *56*, 11945; *Angew. Chem.* **2017**, *129*, 12107.
- [92] J. Krüger, F. Eisenhut, D. Skidin, T. Lehmann, D. A. Ryndyk, G. Cuniberti, F. García, J. M. Alonso, E. Guitián, D. Pérez, D. Peña, G. Trinquier, J.-P. Malrieu, F. Moresco, C. Joachim, *ACS Nano* **2018**, *12*, 8506.
- [93] J. Krüger, F. Eisenhut, J. M. Alonso, T. Lehmann, E. Guitián, D. Perez, D. Skidin, F. Gamaleja, D. A. Ryndyk, C. Joachim, D. Peña, F. Moresco, G. Cuniberti, *Chem. Commun.* **2017**, *53*, 1583.
- [94] J. Krüger, N. Pavliček, J. M. Alonso, D. Pérez, E. Guitián, T. Lehmann, G. Cuniberti, A. Gourdon, G. Meyer, L. Gross, F. Moresco, D. Peña, *ACS Nano* **2016**, *10*, 4538.
- [95] P. Schmitteckert, R. Thomale, R. Korytár, F. Evers, *J. Chem. Phys.* **2017**, *146*, 092320.
- [96] M. J. van Setten, D. Xenioti, M. Alouani, F. Evers, R. Korytár, *J. Phys. Chem. C* **2019**, *123*, 8902.
- [97] W. H. Soe, C. Manzano, A. De Sarkar, N. Chandrasekhar, C. Joachim, *Phys. Rev. Lett.* **2009**, *102*, 176102.
- [98] J. I. Urgel, S. Mishra, H. Hayashi, J. Wilhelm, C. A. Pignedoli, M. Di Giovannantonio, R. Widmer, M. Yamashita, N. Hieda, P. Ruffieux, H. Yamada, R. Fasel, *Nat. Commun.* **2019**, *10*, 861.
- [99] F. Eisenhut, J. Krüger, D. Skidin, S. Nikipar, J. M. Alonso, E. Guitián, D. Pérez, D. A. Ryndyk, D. Peña, F. Moresco, G. Cuniberti, *Nanoscale* **2018**, *10*, 12582.
- [100] M. Zugermeier, M. Gruber, M. Schmid, B. P. Klein, L. Ruppenthal, P. Müller, R. Einholz, W. Hieringer, R. Berndt, H. F. Bettinger, J. M. Gottfried, *Nanoscale* **2017**, *9*, 12461.
- [101] G. Trinquier, G. David, J.-P. Malrieu, *J. Phys. Chem. A* **2018**, *122*, 6926.
- [102] J. I. Urgel, H. Hayashi, M. Di Giovannantonio, C. A. Pignedoli, S. Mishra, O. Deniz, M. Yamashita, T. Dienel, P. Ruffieux, H. Yamada, R. Fasel, *J. Am. Chem. Soc.* **2017**, *139*, 11658.
- [103] H. F. Bettinger, *Pure Appl. Chem.* **2010**, *82*, 905.
- [104] T. Stuyver, B. Chen, T. Zeng, P. Geerlings, F. De Proft, R. Hoffmann, *Chem. Rev.* **2019**, *119*, 11291.
- [105] M. Abe, *Chem. Rev.* **2013**, *113*, 7011.
- [106] K. N. Houk, P. S. Lee, M. Nendel, *J. Org. Chem.* **2001**, *66*, 5517.
- [107] D. Jiang, S. Dai, *J. Phys. Chem. A* **2008**, *112*, 332.
- [108] C. Raghunath, Y. Anusooya Pati, S. Ramasesha, *Phys. Rev. B* **2002**, *66*, 035116.
- [109] D. Casanova, M. Head-Gordon, *Phys. Chem. Chem. Phys.* **2009**, *11*, 9779.
- [110] B. Hajgató, D. Szieberth, P. Geerlings, F. De Proft, M. S. Deleuze, *J. Chem. Phys.* **2009**, *131*, 224321.
- [111] B. Hajgató, M. Huzak, M. S. Deleuze, *J. Phys. Chem. A* **2011**, *115*, 9282.
- [112] H. Chakraborty, A. Shukla, *J. Phys. Chem. A* **2013**, *117*, 14220.
- [113] Y. Gao, C.-G. Liu, Y.-S. Jiang, *J. Phys. Chem. A* **2002**, *106*, 2592.
- [114] J.-D. Chai, *J. Chem. Phys.* **2012**, *136*, 154104.
- [115] J.-D. Chai, *J. Chem. Phys.* **2014**, *140*, 18A521.
- [116] Y. Yang, E. R. Davidson, W. Yang, *Proc. Natl. Acad. Sci. USA* **2016**, *113*, E5098.
- [117] C. U. Ibeji, D. Ghosh, *Phys. Chem. Chem. Phys.* **2015**, *17*, 9849.
- [118] N. Dupuy, M. Casula, *J. Chem. Phys.* **2018**, *148*, 134112.
- [119] J. W. Mullinax, E. Epifanovsky, G. Gidofalvi, A. E. DePrince, *J. Chem. Theory Comput.* **2019**, *15*, 276.
- [120] M. Mostafanejad, A. E. DePrince, *J. Chem. Theory Comput.* **2019**, *15*, 290.
- [121] J. Fosso-Tande, T.-S. Nguyen, G. Gidofalvi, A. E. DePrince, *J. Chem. Theory Comput.* **2016**, *12*, 2260.
- [122] J. B. Schriber, F. A. Evangelista, *J. Chem. Phys.* **2016**, *144*, 161106.
- [123] J.-D. Chai, *J. Chem. Phys.* **2017**, *146*, 044102.
- [124] C.-S. Wu, J.-D. Chai, *J. Chem. Theory Comput.* **2015**, *11*, 2003.
- [125] J. Lee, D. W. Small, E. Epifanovsky, M. Head-Gordon, *J. Chem. Theory Comput.* **2017**, *13*, 602.
- [126] D. H. Ess, E. R. Johnson, X. Hu, W. Yang, *J. Phys. Chem. A* **2011**, *115*, 76.
- [127] H. H. Wenk, M. Winkler, W. Sander, *Angew. Chem. Int. Ed.* **2003**, *42*, 502; *Angew. Chem.* **2003**, *115*, 518.
- [128] J. Shee, E. J. Arthur, S. Zhang, D. R. Reichman, R. A. Friesner, *J. Chem. Theory Comput.* **2019**, *15*, 4924.
- [129] G. Karakostasakis, L. Liu, R. Thomale, S. A. Kivelson, *Phys. Rev. B* **2013**, *88*, 224512.
- [130] M.-H. Whangbo, R. Hoffmann, R. B. Woodward, *Proc. R. Soc. London Ser. A* **1979**, *366*, 23.
- [131] S. Hemmatiyani, D. A. Mazziotti, *J. Phys. Chem. C* **2019**, *123*, 14619.
- [132] L. Crocker, T. Wang, P. Kebarle, *J. Am. Chem. Soc.* **1993**, *115*, 7818.
- [133] M. S. Deleuze, L. Claes, E. S. Kryachko, J. P. François, *J. Chem. Phys.* **2003**, *119*, 3106.
- [134] B. Hajgató, M. S. Deleuze, D. J. Tozer, F. De Proft, *J. Chem. Phys.* **2008**, *129*, 084308.
- [135] J. Wilhelm, M. Del Ben, J. Hutter, *J. Chem. Theory Comput.* **2016**, *12*, 3623.
- [136] J. W. Mullinax, E. Maradzike, L. N. Koulias, M. Mostafanejad, E. Epifanovsky, G. Gidofalvi, A. E. DePrince, *J. Chem. Theory Comput.* **2019**, *15*, 6164.
- [137] W. Mizukami, Y. Kurashige, T. Yanai, *J. Chem. Theory Comput.* **2013**, *9*, 401.
- [138] K. Pelzer, L. Greenman, G. Gidofalvi, D. A. Mazziotti, *J. Phys. Chem. A* **2011**, *115*, 5632.
- [139] J. Fosso-Tande, D. R. Nascimento, A. E. DePrince, *Mol. Phys.* **2016**, *114*, 423.
- [140] S. Lehtola, J. Parkhill, M. Head-Gordon, *Mol. Phys.* **2018**, *116*, 547.

- [141] J. B. Schriber, K. P. Hannon, C. Li, F. A. Evangelista, *J. Chem. Theory Comput.* **2018**, *14*, 6295.
- [142] J.-P. Malrieu, G. Trinquier, *J. Phys. Chem. A* **2016**, *120*, 9564.

- [143] H. Hayashi, N. Hieda, M. Yamauchi, Y. S. Chan, N. Aratani, S. Masuo, H. Yamada, *Chem. Eur. J.* **2020**, *26*, 15079.

Manuscript received: June 30, 2020

Revised manuscript received: August 18, 2020

Version of record online: December 28, 2020
